PREDICTING CHANGES IN SATURATED HYDRAULIC CONDUCTIVITY OF BIORETENTION MEDIA AMENDED WITH BIOCHAR

by

Jing Jin

A thesis submitted to the Faculty of the University of Delaware in partial fulfillment of the requirements for the degree of Master of Civil Engineering

Spring 2016

PREDICTING CHANGES IN SATURATED HYDRAULIC CONDUCTIVITY OF BIORETENTION MEDIA AMENDED WITH BIOCHAR

by

Jing Jin

Approved: ______________________________

Paul T. Imhoff, Ph.D.
Professor in charge of thesis on behalf of the advisory Committee

Approved: ______________________________

Harry W. Shenton III, Ph.D.
Chair of the Department of Civil and Environmental Engineering

Approved: ______________________________

Babatunde Ogunnaike, Ph.D.
Dean of the College of Engineering

Approved: ______________________________

Ann L. Ardis, Ph.D.
Senior Vice Provost for Graduate and Professional Education

ACKNOWLEDGMENTS

I would like to give my sincere gratitude to my favorite professor at the University of Delaware, Dr. Paul Imhoff, for his inspiring advice and ideas in the past two years. It is an honor for me to have the great opportunity to work with him and learn from him. Thank him for being such an exceptional mentor and for buying us Pizza.

I want to express my gratitude to my family for their supports, my progression to this point would have been impossible without their love and encouragements. Many thanks to my lab mates, for their valuable comments, suggestions and help. Additionally, I am particularly grateful to my lovely friends: Mr. Chad Wasileski and Mrs. Gab Wasileski, Haotian Xu, Yiyun Zhu and Sheng Sheng for their kindness and care. My deepest appreciation goes to Haoda Min, for his patience on guiding me with the plots in this thesis.

Finally, I would also like to thank the Delaware Department of Transportation, and National Fish and Wildlife Foundation for providing fundings over the term of my studies.

TABLE OF CONTENTS

Appendix

LIST OF TABLES

LIST OF FIGURES

ABSTRACT

The addition of biochar to soil has been shown to improve soil quality for agronomic applications, demonstrating its usefulness in altering soil physical and chemical properties. While biochar has also been added to stormwater treatment media, little is known about its impact on hydraulic properties, especially the saturated hydraulic conductivity (K_{sat}). The objective of this research was to measure the K_{sat} of stormwater bioretention media with three different sizes of biochar amendment (4% w/w). Based on the K_{sat} results and the physical properties of the biochar and biochar-amended media (i.e. d_{50}, void ratio, etc.), existing models were evaluated for their ability to predict the changes in K_{sat} due to biochar addition.

Soil reef biochar used in this study is a commerically available biochar produced through pyrolysis of softwood cuttings at 550 °C, and it was divided into three groups with different particle sizes: small ($\leq$ 0.841 mm), unsieved, and large (0.841-4.76 mm). The bioretention medium consisted of sand, clay, and sawdust with a percentage of 88%, 8% and 4% (w/w). Addition of these biochars universally decreased dry bulk density and increased the porosity compared to the unamended medium, regardless the biochar particle size. K_{sat} increased for all bioretention media: small biochar caused less increase (67%), and unsieved and large biochar amendment lead to greater increases (306% and 213%). Based on sediment-biochar particle size, porosity, etc., most of the existing models in the literature that predict K_{sat} based upon particle size were able to predict changes in K_{sat} to within an order of magnitude and in the correct direction. Biochar amendments were also tested with a uniform sand. In contrast to the bioretention medium, all biochars decreased K_{sat}. The Kozeny-Carmen model was best at predicting changes in K_{sat}, with the smallest average root mean square error, although this model (and all others) predicted K_{sat} to increase with large biochar

amendment while experiments showed that it decreased. This perplexing result is hypothesized to be associated with the roughness of large biochar particles and the influence of theses large particles on flow path tortuosity. Future work should seek to quantify this effect through X-ray computed tomography measurements.

Chapter 1

INTRODUCTION

Biochar is produced by thermal decomposition of organic matter heated under relatively low temperatures ($\leq 700\,^{\circ}$C) with limited oxygen. As a carbon product, biochar can be derived from biomass such as wood, manure, sludge, etc. However, unlike burning biomass in a fire that creates ash, which mainly contains minerals and inorganic carbonate, biochar is more carbon-rich and is deliberately created for environmentally anthropogenic purposes (Lehmann and Joseph, 2009; Lopez, 2014). Biochar has been widely applied as soil amendments to increase soil crop productivity and potentially the hydrologic properties of the soils. It was found to sequester carbon (Glaser *et al.,* 2002), improve nutrient retention (Laird *et al.,* 2010), and increase soil water holding capacity and available water content (Lehmann and Joseph, 2006). It may also change the soil chemical properties such as pH, cation exchange capacity (Glaser *et al.,* 2002), and soil physical properties such as structural stability and hydraulic conductivity (Barnes *et al.,* 2014).

1.1 Biochar

1.1.1 Production

As feedstock composition and pyrolysis conditions have a significant influence on biochar pore structure, surface area and adsorption capability, its properties are highly dependent on the type of feedstock and pyrolysis process and temperature (Downie *et al.,* 2009). By different degradation mechanisms, the cellular structure of biomass is broken down to cellulose, hemicellulose, lignin, and organic materials. Woods with high lignin contents tend to produce more char than those derived from herbaceous feedstocks. Biochar derived from manure may contain more nutrients such as phosphorus, potassium, and calcium (Bridgwater *et al.,* 1999; Sparkes and Stoutjesdijk 2011). It was also shown that an increase in pyrolysis temperature leads to an increase in C content of the biochar (Laird 2009a).

Methods of biochar production includes slow pyrolysis, flash pyrolysis, gasification, and fast pyrolysis. Slow pyrolysis usually yields approximately 35% biochar, 30% bio-oil, and 35% syngas by mass. Flash pyrolysis can maximize biochar production by heating batches of biomass under relatively high pressure, which typically yields 60% biochar and 40% bio-oil and syngas. A flash pyrolyzer often consists of heat-recovery equipment. Gasification is designed for maximum syngas production, typically with only about 10% or less of biomass and 90% gaseous products. Fast pyrolysis usually employs continuous-flow systems that create primarily bio-oil, usually with 50-70% bio-oil, 10-30% biochar, and 15-20% syngas by mass (Laird 2009b; Meyer *et al.,* 2011).

1.1.2 Biochar Dilemma

In spite of the fact that biochar has been widely recognized as a very useful soil amendment, its negative impacts cannot be ignored. Mukherjee and Lal (2014) discussed several negative aspects of biochar which were seldom reviewed by many researchers. It is known that nutrients such as Phosphate (P) and Nitrogen (N) can be retained in soil with biochar addition due to its high cation exchange capacity (CEC), yet it was found that animal biomass-derived biochar which has a higher pH than plant-derived biochar may adversely affect crops and forest plants, as a result of nutrient deficiency at a higher pH (Xu *et al.,* 2012). Therefore, alteration of pH by biochar may limit availability of soil nutrients and adversely affect soil CEC (Lehmann and Joeseph, 2009).

Biochar is believed to increase soil surface area (SA) due to its highly microporous characteristics. However, research showed that for soil with biochar applications, SA measured by N_2 did not significantly shift compared to a control group. This response was explained by pores clogging due to microbial activity (Mukherjee and

Lal, 2014). Many studies have shown that biochar increases soil aggregate stability. Nevertheless, it was found that an application of 0.5% oak biochar pyrolysed under 650 °C (w/w) on a silty clay loam soil resulted in a 10% decrease in soil aggregation compared to control. In another case, biochar did not affect the aggregate stability at a 1% application rate (Peng *et al.,* 2011). The observations suggest that there might be a threshold application rate in which case either no changes in aggregate stability occur or the stability decreases. In addition, effects of biochar application on greenhouse gas (GHG) emissions have been reported, though the data on effects of biochar application on GHG emissions are inconsistent. Rondon (Rondon *et al.,* 2005) observed a virtually complete suppression of methane emissions of soil at biochar additions of 20 g/kg, while Spokas (Spokas *et al.,* 2009) found that biochar-amended soils can enhance CO_2 and CH_4 emissions due to microbial decomposition.

Another issue with biochar is related to the initial financial investment. Improvements in soil properties such as soil aggregation and soil strength are expected to be observed over a long time period (Hale *et al.,* 2011, Lin *et al.,* 2012). Biochar production is time and labor intensive, and there are still many uncertainties as to the application rate, pyrolysis temperature, and feedstock for both environmental and agronomic improvements. Are the benefits associated with biochar addition significant enough and can they be realized in a short enough time period to warrant the cost of application? To make such decisions it is necessary to understand the mechanisms and effects of biochar application; various soil-biochar combinations in laboratory and field conditions should be tested in the future.

1.2 Stormwater Remediation Application

Biochar has been reported to have high CEC and high SA which enables biochar to absorb cations efficiently. Published data on the CEC of biochar are quite variable, ranging from 71 mmol/kg (Cheng *et al.,* 2008) to 146 cmol/kg (Takaya *et al.,* 2015). SA varies with feedstock and pyrolysis temperature; for example, Laurel oak pyrolysed at 250 °C has a SA of 1 m^2/g, while Loblolly pine heated under 650 °C has a SA of

285 m^2/g (Mukherjee *et al.,* 2011). Biochar's ability to sorb N species has been evaluated to determine the potential in removing NO_3^- from a solution (Yao *et al.,* 2012). Besides N compounds, the presence of biochar plays a critical role in increasing retention of P and thereby reducing nutrient leaching (Lehmann *et al.,* 2003). Biochar also appears to stimulate microbial activity by providing elevated bio-available nutrients including N, P, and metal ions, and it can also serve as a habitat for microbial groups due to its large internal volume (Warnock *et al.,* 2007).

In addition to improving chemical properties, previous studies have illustrated that biochar addition improves soil-water retention and increases saturated hydraulic conductivity (K_{sat}) as a result of its high SA and large internal pore volume (Tian *et al.,* 2014; Herath *et al.,* 2013; Moutier *et al.,* 2000; Oguntunde *et al.,* 2008). Contradictorily, other studies observed reduction in K_{sat} following biochar addition (Lim *et al.,* , 2015; Barnes *et al.,* 2014; Brokhoff *et al.,* 2010). All those previous tests showed that a change in K_{sat} is dependent on the soil type, biochar amendment rate, and biochar properties.

Seeing the benefits brought by biochar amendment for agricultural applications, researchers started to utilize biochar as filtration media in stormwater bioretention system to remove pollutants including total suspended solids, metal ions, nutrients, and microbes (Beck *et al.,* 2011, Reddy *et al.,* 2014). A novel stormwater remediation system with incoporation of 4% wood biochar (w/w) and zero-valent iron has been implemented, with a purpose to enhance the denitrification process and attenuate pollutants, thereby leading to nitrogen load reduction (Tian *et al.,* unpublished). This pilot-scale bioretention system consists of two side-by-side experimental cells. The unmodified cell contains 100% sediment mix while the biochar cell contains 4% biochar and 96% sediment mix by mass. Two pilot-scale experiments were conducted that included a bromide tracer and nitrate as an influent with a hydraulic loading of 5.5 cm/h for 24 h and 36 h in the summer. Tracer tests and time-domain reflectometer (TDR) measurements showed that biochar increased the average volumetric water content of the vadose zone by 14.7% and the mean residence time by 12.6%. For the spring field test at 14 °C, nitrate in the control cell effluent increased by 6.1% but decreased by 43.5% for the biochar cell. For the summer field test at 22 °C, 30.6% and 84.7% of influent nitrate was removed in the control and biochar cells, respectively. In the summer field test, total nitrogen in the influent was decreased by a factor of 5 in the biochar cell effluent and was primarily nitrate and ammonium. Nitrate removal in the medium amended with biochar was enhanced through improved redox conditions (lower gas saturations), longer hydraulic retention time, and increased microbial activity.

1.3 Research Motivation

Part of the work in the stormwater remediation project described above is to examine the effect of biochar addition on K_{sat}. Initially, laboratory K_{sat} for the field media showed that K_{sat} of biochar-amended media increased by a factor of 4 compared to bioretention media without biochar addition. While increasing water infiltration and drainage is advantageous for reducing run-off and flooding in the field, it is also important to retain nutrients from stormwater. In order to understand biochar's effect on K_{sat}, successive K_{sat} measurements using a reliable saturation method were conducted in this study using porous media with different textures and a well-characterized biochar sieved to different particle sizes.

A large number of models have been developed to predict K_{sat} for different soil textures (Kozeny, 1927; Carmen 1937; Hazen, 1892; NAVFAC, 1974; Chapius, 2004; Shahabi, 1984; Fair and Hatch, 1933; Lim *et al.,* 2015). Lim *et al.* (2015) studied four different types of soils, two of which are commercial mixes of silica sand that can be classified as fine sand and coarse sand; while a silt loam and clay loam were natural soils collected from Minnesota. The ranges of particle size of fine sand and coarse sand are approximately between 0.1 to 0.25 mm and 0.15 to 2 mm, respectively; while particles in the silt loam and clay loam ranged from 0.01 to 2 mm. The Lim *et al.* (2015) model utilized four different pedotransfer functions (PTF) based on the clay and sand size fractions. It averaged the results from the four PTFs to obtain estimated K_{sat}, and it accurately predicted the direction of the K_{sat} influence for the biochar amended soils in most cases. The one important exception is that the Lim *et al.* (2015) model was not able to predict the reduction in K_{sat} that occurred when large biochar particles were added to sand media; instead, the Lim *et al.* (2015) model predicted K_{sat} to increase.

While the model developed by Lim *et al.* (2015) was able to successfully predict the change of direction in K_{sat} for many soil samples, the focus in this study is to evaluate current models in predicting K_{sat} changes to bioretention media with biochar amendment. Because bioretention media have high sand content and given the problems encountered in previous modeling efforts to describe the impact of biochar on K_{sat} in such media, the utility of existing models for predicting K_{sat} in such media is an important question.

Chapter 2

BACKGROUND

An important soil properties that controls the transmission of water is the saturated hydraulic conductivity (Klute, 1965). The hydraulic conductivity describes the ease of water movement through porous media and is a function of soil properties (*e.g.,* soil texture, particle size, organic matter content, and overall soil structure) and fluid properties (*e.g.,* fluid saturation, viscosity and density) (Liu *et al.,* 2015). Saturated hydraulic conductivity K_{sat} is a critical parameter in predicting complex water movement and retention pathways through the soil profile (Lim *et al.,* 2015).

Henry Darcy is a French engineer who formulated Darcy's Law based on a number of experiments on the flow of water through sand beds. Darcy's Law is a flux equation describing the flow of water in soils and can be generalized for application between any two points of a saturated porous medium provided that there is a total potential difference between them (Jury, 2004). It is given by

$$Q = \frac{K_s A \Delta H}{L} \tag{2.1}$$

where

Q is the volume of fluid flowing per unit time (L^3/t),

L is the length of saturated packed sand column (L), and

A is the cross sectional area of the packed sand column (L^2).

Equation (2.1) describes the volume of fluid flowing per unit time, Q, through a saturated packed sand column of length L and area A.

2.1 K_{sat} Data from Literature

Previous studies showed inconsistent results of soil biochar additions on K_{sat}; thus, the mechanisms by which biochar alters K_{sat} remain unclear. Researchers have

Table 2.1: Literature K_{sat} of biochar amended soils.

Soil texture	Biochar particle size (mm)	Biochar application rate (%)	Response	Author & year
Sand	<0.18	0∼3%	Decrease	Uzoma *et al.*, (2011)
Sand	<0.85	10%	Decrease	Barnes *et al.*, (2014)
Sand	5∼8	0∼2.5%	Decrease	Zhang *et al.*, (2016)
Sand	0.05∼8	0∼5%	Decrease	Lim *et al.*, (2015)
Sand	∼0.63	0∼10%	Decrease	Ajayi *et al.*, (2016)
Sand	0.251∼0.853	0∼2%	No effect	Liu *et al.*, (2016)
Loamy sand	3.84	∼5%	No effect	Hardie *et al.*, (2014)
Loamy sand	<0.2	0∼10%	Decrease	Pathan *et al.*, (2003)
Loamy sand	< 0.1	30%	Decrease	Ghodrati *et al.*, (1995)
Loam	<2	∼5%	No effect	Lei & Zhang (2013)
Loam	∼1.0	1%	Increase	Herath *et al.*, (2013)
Loam	0.05∼8	0∼5%	No effect	Lim *et al.*, (2015)
Fine loamy	<0.5	0∼2%	No effect	Laird *et al.*, (2010)
Silt loam	∼1.06	0∼3%	No effect	Rogovska *et al.*, (2014)
Sandy loam	< 2	2%	Increase	Ouyang *et al.*, (2013)
Sandy loamy silt	∼0.63	0∼10%	Increase	Ajayi *et al.*, (2016)
Silty Clay	< 2	2%	Increase	Ouyang *et al.*, (2013)
Clay	< 2	1∼3%	Increase	Asai *et al.*, (2009)
Clay	0.25∼0.5	0∼3%	No effect	Kameyama *et al.*, (2012)

.

found that biochar characteristics such as feedstock, pyrolysis temperature, the application rate, and soil characteristics will alter K_{sat} (Barnes *et al.,* 2014). Existing literature studies on the impact of biochar addition on K_{sat} are tabulated in Table 2.1.

As Table 2.1 shows, biochar either decreased K_{sat} or had no impact on sandy soils, but either increased or had no influence on loam, silt, and clay textures. A decrease in K_{sat} for sand can be explained by obstructions in the soil matrix from the biochar particles, which increased the tortuosity of the porous media (Kameyama *et al.,* 2012, Lim *et al.,* 2015). Based on the observation of those literature data, the biochar's effect on K_{sat} for loam, silt, and clay textures depends on biochar particle size, and application rates. However, the mechanism of K_{sat} alteration as a result of biochar size has not been studied extensively. Biochar application is believed to create more interstitial space within the biochar-soil mixture, increasing the porosity and therefore increasing K_{sat} (Barnes, 2014). Additionally, Ouyang *et al.,* (2013) noted that the different results might also be partly attributable to the different characteristics of biochars used (*e.g.,* C/N ratio). A higher C/N ratio is favorable for fungi, in which case an increasing amount of excreted hyphae can lead to an improvement of K_{sat} through aggregate formation (DeGryze *et al.,* 2005). In addition, biochar application expands the available surfaces for the formation of bonds and complexes with ions, which potentially causes further structure stability, thus improving macroaggregate formation, that increases the number of mesopores and thus K_{sat} (Ajayi *et al.,* 2016).

2.2 K_{sat} Models

The K_{sat} value of soils can be either measured or predicted. Most field and laboratory tests are time consuming and costly; therefore a number of models have been developed to predict the K_{sat} of soils, such as Kozeny-Carmen, Hazen Equation, Shahabi, Chapius Formula, etc. (Chapius, 2012; Carrier, 2003). These models do not account for soil aggregate formation, and thus predict the short-term effect of biochar on soils and the effect of biochar on sediments deep in bioretention filter media, where aggregate formation is hindered.

The impact of biochar on soil hydraulic properties has been studied by evaluating K_{sat} with different biochar feedstock, application rates, and soil texture classes (Lim *et al.,* 2015; Glaser *et al.,* 2002). However, soil structure usually changes over time, so that the complex interaction between natural soil and biochar makes it hard to develop a model to accurately predict K_{sat}. As has been mentioned previously, biochar amendment promoted macroaggregate formation in natural soils, which has not been found to be important for bioretention media. Considering that biochar is a non-plastic medium, six predictive methods for non-plastic soils which are deemed to be reliable and accessible were tested using measured K_{sat} and their performances were compared in this study. These models are described next.

2.2.1 Kozeny-Carmen (K-C)

The Kozeny-Carmen equation (K-C) for hydraulic conductivity was developed by both Kozeny and Carmen's independent work (Kozeny, 1927; Carmen 1937; Wyllie and Gardner, 1958). K-C can be described as:

$$K_{sat} = C\frac{g}{\mu_w \rho_w}\frac{e^3}{S_S^2 G_s^2 (1+e)} \tag{2.2}$$

where

C is a dimensionless constant depending on the pore structure,

g is the gravitational constant (m/s^2),

μ_w is the dynamic viscosity of water (Pa·s),

ρ_w is the density of solids (kg/m^3),

G_s is the specific gravity of solids (G$_s$=ρ_s/ρ_w),

S_s is the specific surface area (m^2/kg), and

e is the void ratio.

Initially, this model was developed by Kozeny to test for industrial powders, and later Carmen modified the model to be used for soil, sand and clay.

2.2.2 Hazen

The Hazen equation was initially developed by Hazen for infiltration systems, which are engineered systems that allow accumulated runoff water to percolate into the subsoil (Hazen, 1892). In many textbooks it is written as:

$$K_{sat} = A(d_{10})^2 \tag{2.3}$$

Equation (2.3) is not the true Hazen equation. Note that the unit of K_{sat} is in cm/s and d_{10} is in mm; A is a constant considered to be 1 at 10 °C. The original equation of Hazen is

$$q = c(d_{10})^2 \frac{h}{L}(0.70 + 0.03T) \tag{2.4}$$

where

q is the Darcy velocity (m/day),

c is a dimensionless constant experimentally indicating close to 1000,

d is the effective size of sand grain, usually d_{10} is used (mm),

L is the length of soil sample through which water passes (m),

h is the hydraulic head loss along distance L(m), and

T is the water temperature (°C).

In this study, the simplified Hazen equation was used and is expressed as (Chapius, 2004):

$$K_{sat} = 1.157 \left(\frac{d_{10}}{1mm}\right)^2 \left[0.70 + 0.03t\left(\frac{T}{1\,^{\circ}\mathrm{C}}\right)\right] \tag{2.5}$$

In laboratory tests, the reference temperature is approximately 23 °C, thus the equation can be simplified to:

$$K_{sat} = 1.60823(d_{10})^2 \tag{2.6}$$

Typically, Hazen applies to loose uniform sands with a uniformity coefficient C_U (d_{60}/d_{10}) $\leq$5 and a grain size d_{10} between 0.1 and 3 mm. Here K_{sat} is in cm/s, and d_{10} is in mm.

2.2.3 NAVFAC

The Navel Facilities Engineering Command design manual DM7 (NAVFAC, 1974) provides a chart to estimate the K_{sat} of clean sand and gravel as a function of void ratio and d_{10}. According to the NAVFAC chart, there is a linear relationship between $\log(K_{sat})$ and $\log(d_{10})$ and this chart can be reduced to a simple equation by solving for the coefficient and the exponent (Chapius *et al.,* 1989).

$$K_{sat} = 10^{1.291e-0.6435}\,(d_{10})^{10^{0.5504-0.2937e}} \tag{2.7}$$

where e is the void ratio and d_{10} is the particle size at which 10% of particles will pass through (mm). Note that here K_{sat} is in cm/s and d_{10} is in mm. Good predictions, which fall between three times and two- thirds the average value, can be achieved when $0.3 \leq e \leq 0.7$, $0.1 \leq d_{10} \leq 2$mm, $2 \leq C_U \leq 12$ and $d_{10}/d_5 \leq 1.4$ (Chapius, 2014).

2.2.4 Chapius

By incorporating Kozeny-Carmen equation and Hazen equation, Chapius plotted K_{sat} vs. the term $d_{10}^2 e^3/(1-e)$ and he then obtained a power-law model by fitting the parameters using experimental data (Chapius, 2004):

$$K_{sat} = 2.4622\left(\frac{d_{10}^2 e^3}{1+e}\right)^{0.7825} \tag{2.8}$$

Similarly to previous equations, K_{sat} is in cm/s and d_{10} is in mm. Chapius states that good predictions (usually within a factor of two)) can be obtained for natural soils with $0.003 \leq d_{10} \leq 3$mm and $0.3 \leq e \leq 1$. Compared with Hazen equation and NAVFAC, for the same set of laboratory data, Chapius equation is the best predictive equation for this experimental data.

2.2.5 Shahabi

Shahabi (Shahabi, 1984) took a natural sand sample from the field and then the soil fractions were mechanically mixed in different proportions to obtain twenty samples. A constant head permeability test on each sample was conducted and K_{sat}

was found to be a function of the effective particle size, uniformity coefficient, and void ratio.

$$K_{sat} = 1.2C_U^{0.735}d_{10}^{0.89}\frac{e^3}{1+e} \tag{2.9}$$

where C_U, d_{10} and e have been defined previously.

The unit of K_{sat} and d_{10} in the above equation are cm/s and mm, respectively. This equation was used for sand specimens and is valid for samples where $1.2 \leq C_U \leq 8$, $0.15 \leq d_{10} \leq 0.59$m, and 0.38$\leq e \leq$0.73 (Chapius, 2014).

2.2.6 Fair-Hatch

Based on dimensional consideration and experimental verification, Fair and Hatch (Fair and Hatch, 1933) developed the following equation of estimating hydraulic conductivity (Bear, 1979).

$$K_{sat} = \frac{\rho_w g}{\mu_w}\frac{1}{A}\left[\frac{(1-\phi)^2}{\phi^3}\left(\frac{B}{100}\sum_{i=1}^{n-1}\frac{F}{d_{m_{i,i+1}}}\right)^2\right]^{-1} \tag{2.10}$$

where

A is a dimensionless packing factor found to be approximately 5,

ϕ is porosity,

B is a particle shape factor equal to 6 for spherical partiles and 7.7 for highly angular ones,

F is the percent by weight of the sample between two successive sieve sizes,

d_m is the geometric mean of the particle sizes between sieve No. i and No. $i+1$, and

n is the total number of sieves.

ρ_w, g and μ_w have been previously.

This formula was initially developed to see fundamental factors governing the flow of water through sand; later it began to be used in estimating permeability from grain size distribution.

Chapter 3

MATERIALS AND METHODS

3.1 Overview of Sediment and Biochar

Eight types of sediment samples were used in this study following the order from "Type 1" to "Type 8". Type 1 and Type 5 are the "control" media without biochar and the remaining are the "modified" group with biochar addition. Soil reef biochar (The Biochar Co., Berwyn, PA) produced through pyrolysis of Southern Yellow hardwood chips at 550 °C was used in this study (referred as "biochar" for simplicity). The biochar batch was purchased in Summer 2014 and was stored in open buckets under room temperature. All measurements and tests were performed starting on February, 2015.

Table 3.1 and 3.2 describes all sediment types in mass percentage (w/w). Type 1 is a sediment mixture including 88% C33 concrete sand (d_{50}: 0.595 mm) (Mason-Dixon Sand & Gravel, Port Deposit, MD), 8% clay (Mason-Dixon Sand & Gravel, Port Deposit, MD), and 4% sawdust (roughly between 0.2 to 1 mm by visual observation) (Second Chance Hardwoods, Elkton, MD) by mass, or 62% C33 sand, 11% clay, and 27% sawdust by volumes bulk volume. Types 2 to 4 consist of 96% Type 1 and 4% biochar with different particle sizes (w/w). 30/40 sand, noted as "Type 5" sample, is a commercial Accusand that has been pre-sieved between #30 (0.595 mm) and #40 (0.4 mm) mesh (d_{50}: 0.541 mm) (Unimin, Pittsburgh, PA). Types 6 to 8 consist of 96% Type 5 and 4% biochar with different particle sizes (w/w). The biochar was classified into three categories: small (<0.841 mm), unsieved, and large (0.841∼4.76 mm). The pictures showing soil reef biochar with different sizes, and Types 1, 3, 5, and 8 can be found in Appendix A. Table B.1 lists biochar's physicochemical properties tabulated by Dr. Pei Chiu's research group at the University of Delaware.

Table 3.1: Sediment samples used in this study.

Type No.	Sample type	Biochar % (w/w)	Biochar size (mm)
1	Bioretention media	0	-
2	Bioretention media	4	<0.841
3	Bioretention media	4	unsieved
4	Bioretention media	4	0.841–4.76
5	30/40 Accusand	0	-
6	30/40 Accusand	4	<0.841
7	30/40 Accusand	4	unsieved
8	30/40 Accusand	4	0.841–4.76

3.2 Biochar Physical Properties

3.2.1 Biochar Density and Porosity

3.2.1.1 Envelope and Skeletal Density

Envelope or particle density (ρ_e) is defined as "the ratio of the mass of a particle to the sum of the volumes including the solid in each piece and the voids within close-fitting imaginary envelopes completely surrounding each piece" (ASTM, 2013). Envelope density is usually very low and as shown in Figure 3.2, it accounts for external voids including both open and closed pores.

Skeletal density is described as "the sample mass divided by the sample skeletal volume, where skeletal volume is the volume occupied by the solid sample" (Brewer, 2014). In this study, mercury porosimetry was chosen to evaluate envelope and skeletal density of biochar samples. Mercury is a non-wetting liquid that can be forced to enter a pore under external pressure. A mercury porosimeter can track the volume of mercury intruded into biochar from minimum to maximum pressures, with the injected volume at each pressure step providing information on the number of pores that might be filled (or drained) at this pressure (Webb, 2001).

Biochar samples were sent to Micrometrics Analytical Services (Norcross, GA) to obtain mercury porosimetry intrusion data. They were first rinsed using DI water for 3-4 times at a ratio of 1:50 at 50 rpm for at least 3 days until the electrical conductivity was less than 100 μm/cm. Then biochars were dried at 105 °C for 12-15 hrs before

Table 3.2: Sample information

Sample	Size range (mm)	Envelope density (g/mL)	Source
Small biochar	0.020-0.841	0.572[a]	The Biochar Co., Berwyn, PA.
Unsieved biochar	0.020-4.76	0.572[a]	The Biochar Co., Berwyn, PA.
Large biochar	0.841-4.76	0.572[a]	The Biochar Co., Berwyn, PA.
C33 sand	0.074-4.76	2.654	Mason-Dixon Sand & Gravel Port.
Clay	N/A	2.845	Mason-Dixon Sand & Gravel Port.
Sawdust	0.2-1[b]	0.25[c]	Second Chance Hardwoods, Elkton MD.
30/40 Accusand	0.4-0.595	2.65	Unimin, Pittsburgh, PA.

[a] The envelope density is measured through mercury porosimitry for biochars sieved between 0.5 to 0.595 mm.
[b] Determined by visual observation.
[c] Information derived from Maharani *et al.*, 2010.

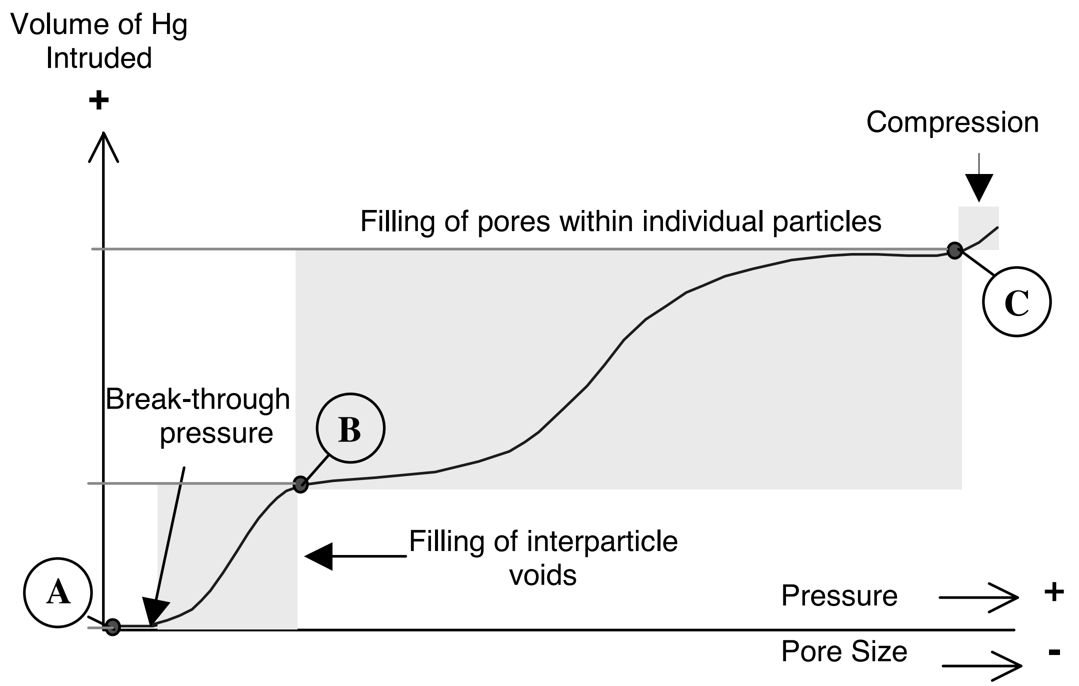

Figure 3.1: Critical points during the mercury intrusion process (Webb, 2001). (Copyright owned by Micromeritics Instruments. Information or figures may not be reproduced or used in any manner without written permission of Micromeritics.)

cooling them to room temperature, followed by a sieving process between #30 (0.595 mm) to #35 (0.5 mm) before analysis. (This work was done by Susan Yi, who is a PhD candidate under Dr. Paul Imhoff's research group).

The critical points during the mercury intrusion process are illustrated in Figure 3.1. The point where the break-through pressure at (as the arrow points to) is used to determine envelope volume, and that break-through point between point B and point C are used to determine inter-particle void volume and skeletal volume, respectively (Webb, 2001).

Figure 3.2 illustrates various volume types. The container on the top left represents characteristics of bulk volume where interparticle and "external" voids are included. The top right is a single porous particle. Black areas shown in the bottom left images represent volumes. The three illustrations at the bottom right in Figure

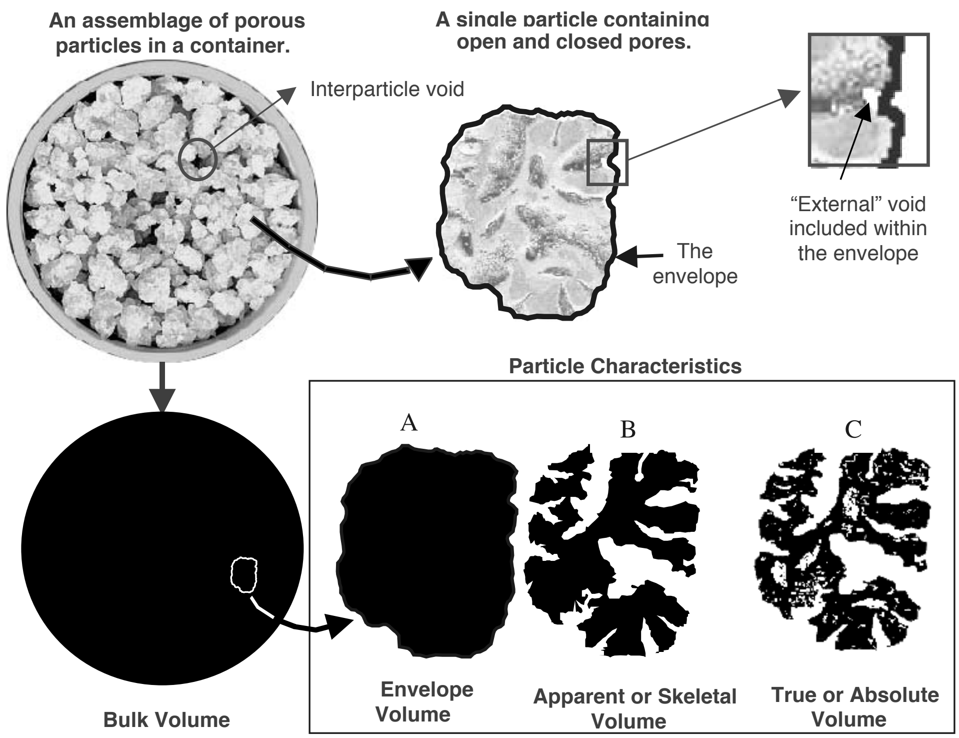

Figure 3.2: Biochar density classes (Webb, 2001). (Copyright owned by Micromeritics Instruments. Information or figures may not be reproduced or used in any manner without written permission of Micromeritics.)

3.2 illustrate the volumes used to determine the envelope, skeletal, and absolute particle densities. Illustration A depicts the volume within the envelope, B is the skeletal volume, and C is the absolute volume and contains on solid material (Webb, 2001).

3.2.1.2 Biochar Porosity

The porosity of biochar represents the ratio of the volumes of the pores in the particles to the volumes enclosed by their envelopes. It can be calculated by (Brewer, 2014)

$$\phi = 1 - \frac{\rho_e}{\rho_s} \tag{3.1}$$

where ρ_e stands for envelope density and ρ_s refers to skeletal density illustrated above. Inter-particle porosity and intra-particle porosity are two forms of porosities for biochar. The term "inter" represents void space between particles and "intra" refers to all porosity within the envelopes of individual particles (Webb, 2001).

Density and porosity of biochar are fundamental physical properties that affect its use as a soil amendment and its potential movement in the natural environment. Biochar is less dense and more porous than soil particles, and the wide range of internal biochar pore sizes (*e.g.,* at least five orders of magnitude) complicates biochar porosity characterization, making it difficult to characterize (Brewer *et al.,* 2014).

Biochar pore volume can be measured by several methods, such as gas sorption (*e.g.,* carbon dioxide adsorption and nitrogen adsorption) (Sing, 1985), mercury porosimetry and stereological methods (*e.g.,* scanning electron microscopy and computerized tomography) (Weibel, 1966). Mercury porosimetry can provide pore characterization with a wide range from a few nanometers to a few hundred micrometers in diameter. However, there are some disadvantages with using this method, including the possibility of sample breakage at high pressures and the inability to distinguish between inter-particle and intra-particle porosity (Brewer *et al.,* 2014).

3.2.2 Biochar Particle Size Distribution

Particle size distribution (PSD) tests for all soil types, including biochars of different sizes, were performed using a mechanical shaker. A number of fine particles were found in the biochar sample; thus, besides a manual sieve analysis test, a hydrometer test was conducted in order to gain a complete size distribution curve of the biochar sample.

According to the standard procedure described by ASTM for manual sieving (ASTM, 2014), at least 200 g of biochar samples were placed on the mechanical shaker followed by a 15 min agitation, with sieves No. 4, 10, 14, 30, 70, 100, 200 and 450. A hydrometer test involved a dispersion process of the sample that passed sieve No. 200 (retained on sieve No. 450 and the bottom pan), followed by taking hydrometer readings at 2, 5, 10, 15, 30, 60, 250 and 1440 min (ASTM, 2007). (The hydrometer test was performed by Ali Nakhli, who is a PhD candidate in the Environmental Engineering Department under the supervision of Dr. Paul Imhoff).

3.3 Sediment Physical and Chemical Properties

3.3.1 Sediment Porosity and Density

In soil science, soil bulk density is defined as the mass of the particles divided by the volume they occupy including the space between the particles (ASTM, 2013). Soil bulk density is an indicator of compaction in a soil and is a reflection of soil structure for water flow and aeration (Lopez, 2014). Soil bulk density largely depends on how it is handled. In this study, a chromatography column (Ace Glass, NJ) was packed with the sediments rather than a intact core from the field to determine the bulk density. All samples were dried in an oven at 105 °C for at least 24 hours before packing. The glass column is 30 cm in length and 5 cm in diameter, and dried soil samples were packed into it by tapping down 10-15 times with a 1 cm I.D. stick for every 1-2 cm soil segment. The top layer was flattened by a small spatula to level off the soil particles. Bulk density was calculated by

$$\rho_b = \frac{m_{dry}}{v_{column}} \tag{3.2}$$

where m_{dry} is the mass of dry soil and v_{column} is the inside volume of column.

As introduced in the beginning of this Chapter, Type 1 consists of 88% C33 concrete sand (ρ_e = 2.654 g/ml), 8% clay (ρ_e = 2.654 g/ml), and 4% sawdust (ρ_e = 0.250 g/ml). An integrative mass-weighted particle density for Type 1 was calculated from each of the component's particle density based on their mass fractions, which turns out to be 1.921 g/ml.

Total pore volume was determined by weighing the columns before and after saturating with water, and the difference is total mass of water filling into the soil pores, which divided by the water density provides the total pore volume of each packing. Intra-particle volumes were calculated from the mercury porosimetry data for biochar alone, where it was assumed that the intra-particle pore volume for the sediments was negligible. Subtracting the intra-particle pore volume for the mass of biochar in the column from total pore volume is the inter-particle volume, which can then be used to calculate the inter-particle porosity.

3.3.2 Sediment Particle Size Distribution

PSD measurement were conducted for Types 1 to 5, following a similar procedure described for biochar. The sieve openings for Types 1 to 4 ranged from 0.074 to 4.76 mm, but only ranged between 0.21 to 2 mm for Types 5 to 8 because of the relatively narrow range of particle sizes. No hydrometer test was performed for sediment types. For Types 6 to 8, a volume based PSD was calculated based on PSD of pure biochar and pure sand (see Chapter 4).

3.3.3 Sediment pH

Soil pH is an important property that characterizes the acidity and alkalinity of soil, and it can be used to determine the mineral solubility and ion mobility. pH influences plant growth, since nutrient and water availability are affected by pH. Soil pH was measured following standard procedures (ASTM, 2007).

3.4 Saturated Hydraulic Conductivity

Considering the relatively high permeability of the tested samples, K_{sat} was measured in the laboratory using the constant head method and a disk infiltrometer was employed to evaluate K_{sat} in the field.

3.4.1 Laboratory Measurements

3.4.1.1 Traditional Saturation Method

To evaluate if biochar-amended columns required special treatment to achieve full water saturation, a simple test with a small column using a traditional saturation method was performed using Types 1, 3, 5, and 7 media. The saturation process was modified following the standard constant head method for measurement of conductivity (Klute, 1965). The column (1 cm in I.D, 8.5 cm in length) was packed with a soil sample using the same packing method described in the above section and was then submerged under de-aired DI water and was soaked for at least 16 hours. The porosity data were then used to compare with the results obtained by an alternative saturation method depicted below.

3.4.1.2 Alternative Saturation Method

As biochar is very porous and often hydrophobic (Yi, et al. 2015), saturating mixtures of biochar and sediment may require special techniques. The chromatography glass columns used in this study have two PTFE column fittings, one on each end. To support uniform flow in the columns, the fittings were drilled and tapped to create a dead zone of approximately 63 mL. Cloths are then glued to the ends to prevent soil particles moving into the dead zone. According to Oliviera *et al.,* (1996) to produce a homogeneous packing of sands, the best dry technique involves the deposition of 0.2-cm layers followed by compaction with a metal pestle. Considering that biochar particles are porous and very fragile, we chose to pack the media in 1-cm increments, using a pestle to gently tamp the top of each 1-cm segment before adding more sediment.

Sediment samples were dried at 105 °C for 24 hours and then were put in a desiccant to cool to room temperature before packing. After the packing process, the following procedure is used to fully saturate the column with water:

1. Column is flushed upward with CO_2 gas for at least 0.5 hours at a flow rate of approximately 30 ml/min to clear out the air; the gas flow rate was low enough to avoid disturbing the soil structure.

2. Close the top of the column and disconnect CO_2 line. Care must be taken during disconnection as air might get into the column easily.

3. Immediately connect the column with tubing filled with de-aired DI water and pump at a constant influent at 0.2 ml/min. The DI water injected into the column should be de-aired with DO level less than 0.5 mg/L. Pump at least 2 pore volumes of de-aired DI water through the column to achieve complete water saturation; this exercise should dissolve entrapped gas bubbles. Depending on the packing of the medium, this process may take 2-3 days to achieve full saturation.

4. If there are visible air bubbles on the inner wall after 2-3 pore volumes, increase the flow rate to dissolve the air bubbles, maintaining the porous medium Reynolds Number less than 1.0.

3.4.1.3 K_{sat} Measurement

The experimental set-up for the saturated hydraulic conductivity experiments is shown in Figure 3.3. Notice that when performing K_{sat} measurements, head loss created by connections of the system may affect the results. Therefore, frictional losses should be minimized by careful selection of tubings and fittings.

Generally there are two types of permeability test methods: the constant head method and the falling head method. Because of a relatively high permeability of the medium involved in this study ($> 10^{-4}$ cm/s), the constant head test method was used to evaluate the K_{sat} results. A peristaltic pump was utilized to create a constant head at different inflow rates.

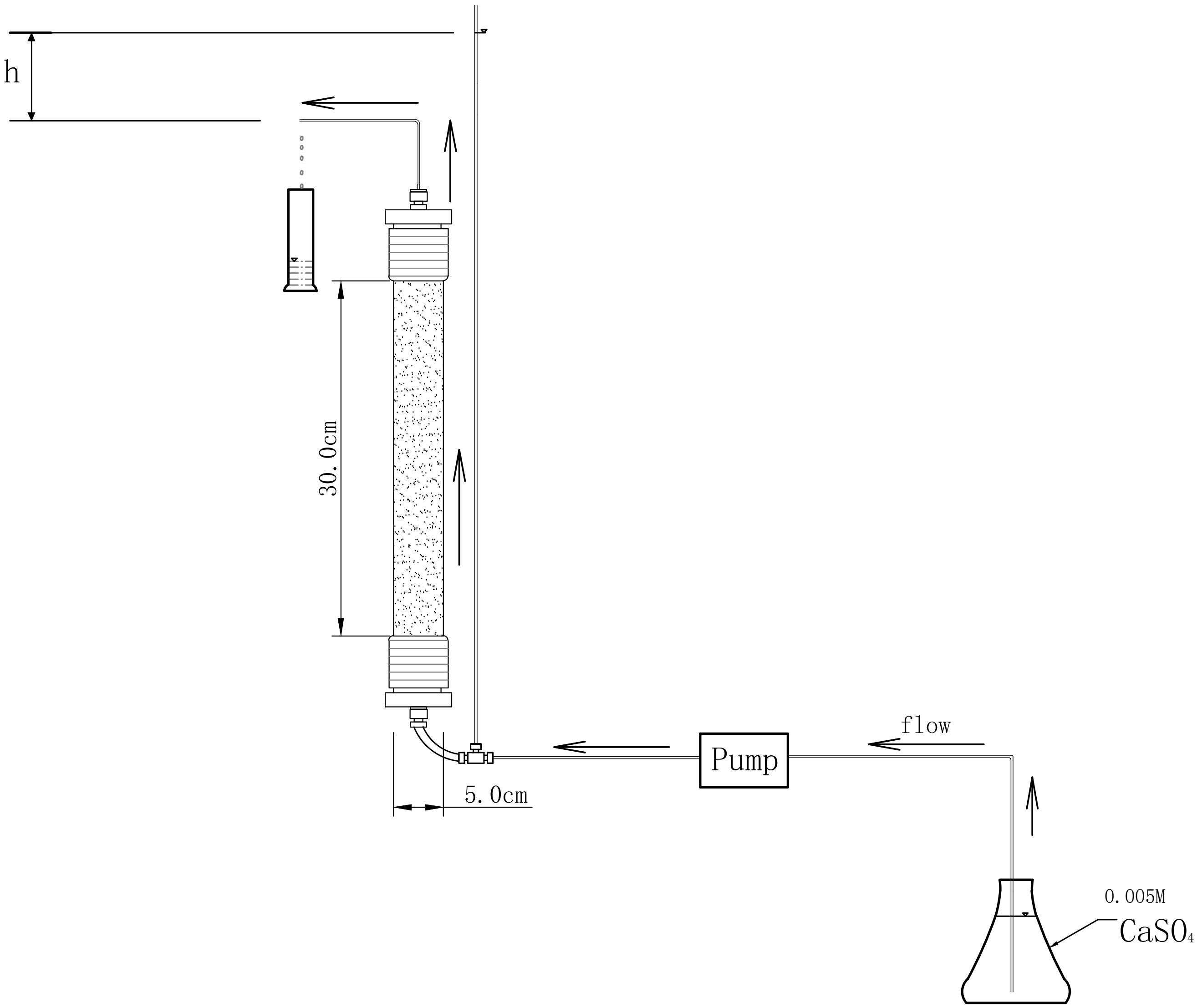

Figure 3.3: Set-up for K_{sat} measurement.

The analysis of K_{sat} using the constant-head method is based on Darcy's law which can be written as:

$$K_{sat} = \frac{Q \times L}{A \times \Delta h} \tag{3.3}$$

where

Q is the steady-state volumetric flow rate (cm^3 s^{-1}),

A is the cross-sectional area perpendicular to flow (cm^2),

L is the effective length of the column excluding length of threads (cm), and

Δh is the head difference between the top and bottom of the porous medium (cm).

Laboratory determination of K_{sat} requires careful measurement of Q and Δh (Madsen *et al.,* 2007). Hydraulic heads were measured using a ruler accurate to 0.1 cm. Flow rate was determined weighing the mass of water collected from the outlet tubing over a specified measurement time. Temperature and electric conductivity were recorded during each test; an averaged value for temperature was used in correcting the K_{sat}. The electric conductivity did not vary dramatically throughout the experiments, thus the effects can be neglected.

For each sediment types, three separate columns were packed, and the K_{sat} for each column was calculated by averaging K_{sat} at different flow rates. A final K_{sat} was determined by averaging it from the three independent columns.

3.4.2 Field Infiltrometer Test

Besides laboratory measurements, the hydraulic conductivity was also evaluated by performing a field infiltrometer test (Following the protocol prepared by Dr. Paul Imhoff, see Appendix C) and modeled by DISC (U.S. Salinity Laboratory, 2000). The infiltrometer tests were performed for Type 1 and 3 in the field located on North Campus at the University of Delaware on June 29, 2015. Two core samples for each Types were taken before and after the test, and were then used to measure the volumetric water content in laboratory. (This test was performed with assistance of Haotian Xu, a master student from Civil &Environmental Engineering Department).

DISC is a computer software package for estimating the unsaturated soil hydraulic properties from tension disc infiltration data and related information. An infiltrometer is a field measurement device for determining soil hydraulic properties (Šimůnek and van Genuchten, 2000). Tension infiltration data were used to measure the K_{sat} using a single disc diameter but with multiple tensions.

DISC code numerically solves the Richards' equation in terms of the van Genuchten equation for saturated-unsaturated water flow. Richard's equation requires information on the volumetric water content, $\theta(h)$, and unsaturated hydraulic conductivity, $K(h)$, where h is the soil-water pressure head. This numerical analysis involves Richard's equation coupled with Levenberg-Marquardt nonlinear minimization method and the governing flow equation is given by:

$$\frac{\partial \theta}{\partial t} = \frac{1}{r}\frac{\partial}{\partial r}\left(rK\frac{\partial h}{\partial r}\right) + \frac{\partial}{\partial z}\left(K\frac{\partial h}{\partial z}\right) - \frac{\partial K}{\partial z} \tag{3.4}$$

where θ is the volumetric water content, K is the hydraulic conductivity, r is a radial coordinate, z is the vertical coordinate and t is time. The Richard's equation is combined with van Genuchten equation:

$$S_e\left(h\right) = \frac{\theta\left(h\right) - \theta_\tau}{\theta_S - \theta_r} = \frac{1}{\left(1 + |\alpha h|^n\right)^m} \tag{3.5}$$

where S_e is the effective fluid saturation, θ_r and θ_s denote the residual and saturated water contents, respectively; l stands for the pore-connectivity parameter and α, n, and $m = 1 - 1/n$ are empirical parameters. The results from DISC will be discussed in Chapter 4.

Chapter 4

RESULTS AND DISCUSSION

4.1 Biochar Physical Properties

4.1.1 Biochar Density and Porosity

Table 4.1 listed the envelope and skeletal densities from mercury porosimetry test. Densities for poultry liter biochar (PLBC) are also listed here for comparison, and SRBC indicates soil reef biochar used in this study.

Table 4.1: Biochar densities and intra-particle pore volume from mercury intrusion porosimetry. The values after ± indicate standard error.

Sample Type	Envelope density, g/mL	Skeletal density, g/mL	Intra-particle pore volume, ml/g
Rinsed PLBC [a]	0.963±0.007	1.719±0.035	0.580±0.009
Rinsed SRBC [b]	0.572±0.002	1.387±0.028	1.066±0.061

[a] PLBC: poultry liter biochar
[b] SRBC: soil reef biochar

The results indicate that SRBC has smaller envelope and skeletal densities than PLBC, and its more porous structure result in a larger intra-particle pore volume.

4.1.2 Biochar Particle Size Distribution

The PSD for three different sizes of biochar were plotted in Figure 4.1. The d_{50} for small, unsieved and large biochar is approximately 0.14, 0.69, and 1.58 mm, respectively. From the small biochar curve, it can be seen that there is indeed a significant amount of fine particles in soil reef biochars. PSD characterization indicates that for unsieved biochar, the particle size ranges from 0.02 to 4.76 mm.

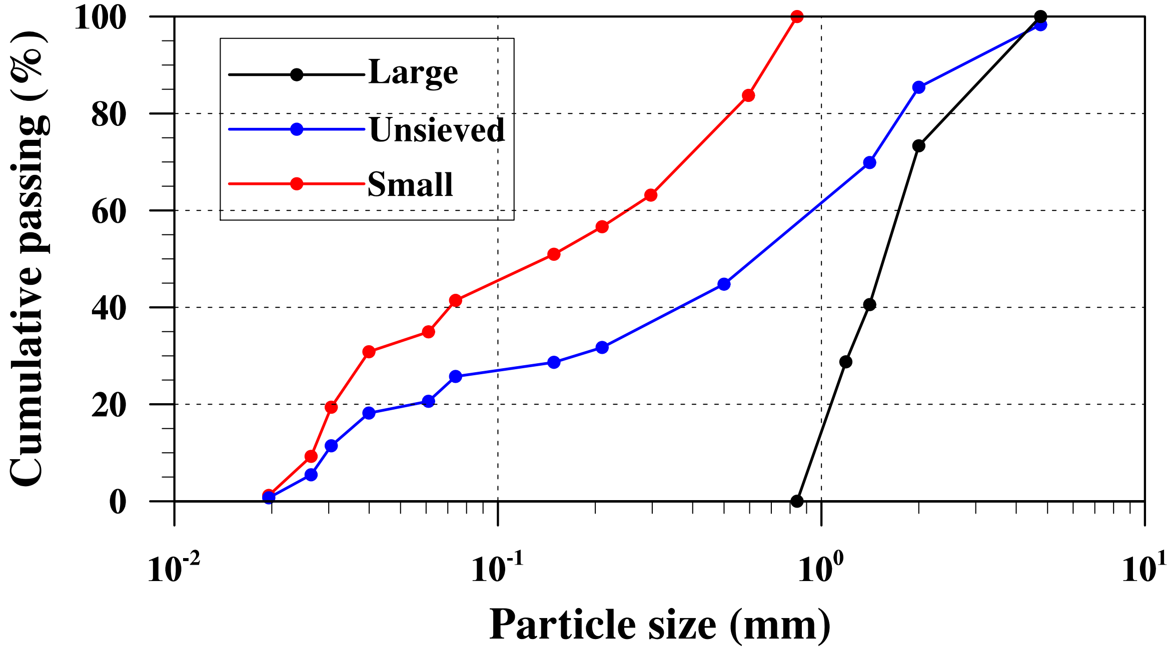

Figure 4.1: Biochar PSD of three different sizes.

4.2 Sediment Physical and Chemical Properties

4.2.1 Sediment Porosity and Density

Table 4.2 lists the porosity data, including intra- and inter- particle porosity, and total porosity for Types 1 to 8, where inter-particle porosities were computed by subtracting intra- particle porosity from total porosity. Biochar increased total porosity for all modified types compared to the control group, and the increased total porosity became larger following larger-size-biochar addition.

4.2.2 Sediment Particle Size Distribution

As biochar and sediment sampels have different envelope densities, the mass based PSD will not be a true reflection of the volume distribution of particles. Instead of plotting the cumulative mass distribution in terms of direct measurements, the cumulative volume distribution should be calculated based on biochar envelope density and average sediment envelope (particle) density. In this case, the biochar or sediment

Table 4.2: Total, and intra- and inter-particle porosity for Types 1-8 [a] media.

Type No.	Total ϕ		Intra-particle ϕ		Inter-particle ϕ	
	-	S.D.	-	S.D.	-	S.D.
1	0.424	3.51e-3	0	0	0.424	3.51e-3
2	0.505	3.51e-3	0.053	1.15e-3	0.451	3.79e-3
3	0.512	3.72e-3	0.055	3.75e-4	0.457	4.09e-3
4	0.581	9.15e-3	0.044	8.57e-4	0.537	1.00e-2
5	0.333	3.55e-3	0	0	0.333	3.55e-3
6	0.398	2.50e-2	0.065	1.15e-3	0.332	2.98e-3
7	0.438	1.66e-2	0.060	1.00e-3	0.378	2.42e-2
8	0.535	4.67e-2	0.050	1.41e-2	0.485	1.48e-2

.

[a] Results were calculated from three samples of Types 1 to 7, and two samples of Type 8.

volume retained on each sieve was converted from mass percentage to volume according to their density and mass fractions, and the mixed cumulative percent passing was summed up after the volume percentage retained on each sieve was calculated. Following this method, the volume based PSDs were plotted for Types 6 to 8. Due to lack of pure clay sample, we were not able to perform a hydrometer test for it, thus for Types 2 to 4, the mass based PSDs were plotted based on mechanical sieve analysis.

Biochar has a smaller envelope density (0.572 g/ml) and a smaller d_{10} (0.027 mm) than Type 1 (1.921 g/ml, 0.228 mm), thus compared to mass based PSD, biochar will lower the d_{10} for the mixtures after converting to volume based PSD (Figure 4.2).

Adding biochar shifted PSD for Types 2 to 4 and Types 6 to 8 (Figure 4.2). The curve for Type 2 was shifted leftward as a result of smaller biochar amendment, and the curve for Type 4 was shifted rightward because of larger biochar addition. For Types 1 to 4, the cumulative passing was not 100% because some particles did not pass through the largest sieve. For Types 6 to 8, d_{50} did not change between sediment types; however, d_{10} became smaller for small and unsieved biochar addition. d_{50} for all types are tabulated in Table D.1.

Figure 4.3 compares the PSD of each ”control” porous medium and unsieved biochar. d_{50} follows an increasing order from unsieved biochar to Type 1, and it is clear to see that unsieved biochar had more fine particles than the control group. Similarly to Type 1, the cumulative passing for biochar did not reach 100% because the big particles did not pass through the largest sieve. (A portion of the PSD tests were done by Kokeb Abera and Yudi Yan, master students from Civil and Environmental Engineering Department.)

4.2.3 Sediment pH

Triplicated samples were tested with DI water and 0.01M $CaCl_2$. The soil pH for only Type 1 and Type 3 were measured, and the results are shown below in Table 4.3.

Table 4.3: pH for Type 1 and Type 3 media.

	DI Water		0.01M $CaCl_2$	
	Type 1	Type 3	Type 1	Type 3
Avg.	4.87	7.88	4.23	7.42
S.D.	0.04	0.06	0.04	0.04

Biochar amendent helped to increase the sediment pH in Type 3 compared to Type 1. The pH measured in DI water is relatively larger than in $CaCl_2$ solution for both types, which is consistent with previous findings, that the pH measured in water is about 0.5 unit higher than that measured in 0.01M $CaCl_2$ (Kalra and Maynard, 1991).

4.3 Saturated Hydraulic Conductivity

4.3.1 Laboratory Measurements

4.3.1.1 Traditional vs. Alternative Saturation Method

Images for water saturation using the alternative method are shown in Figure 4.4. The samples are: (a) Type 1 after 20-min saturation time, (b) Type 3 after 24-hr saturation time, (c) Type 5 after 16-hr saturation time, and (d) Type 7 after 24-hr saturation time. It is obvious to see Type 1 and Type 5 are saturated very well using

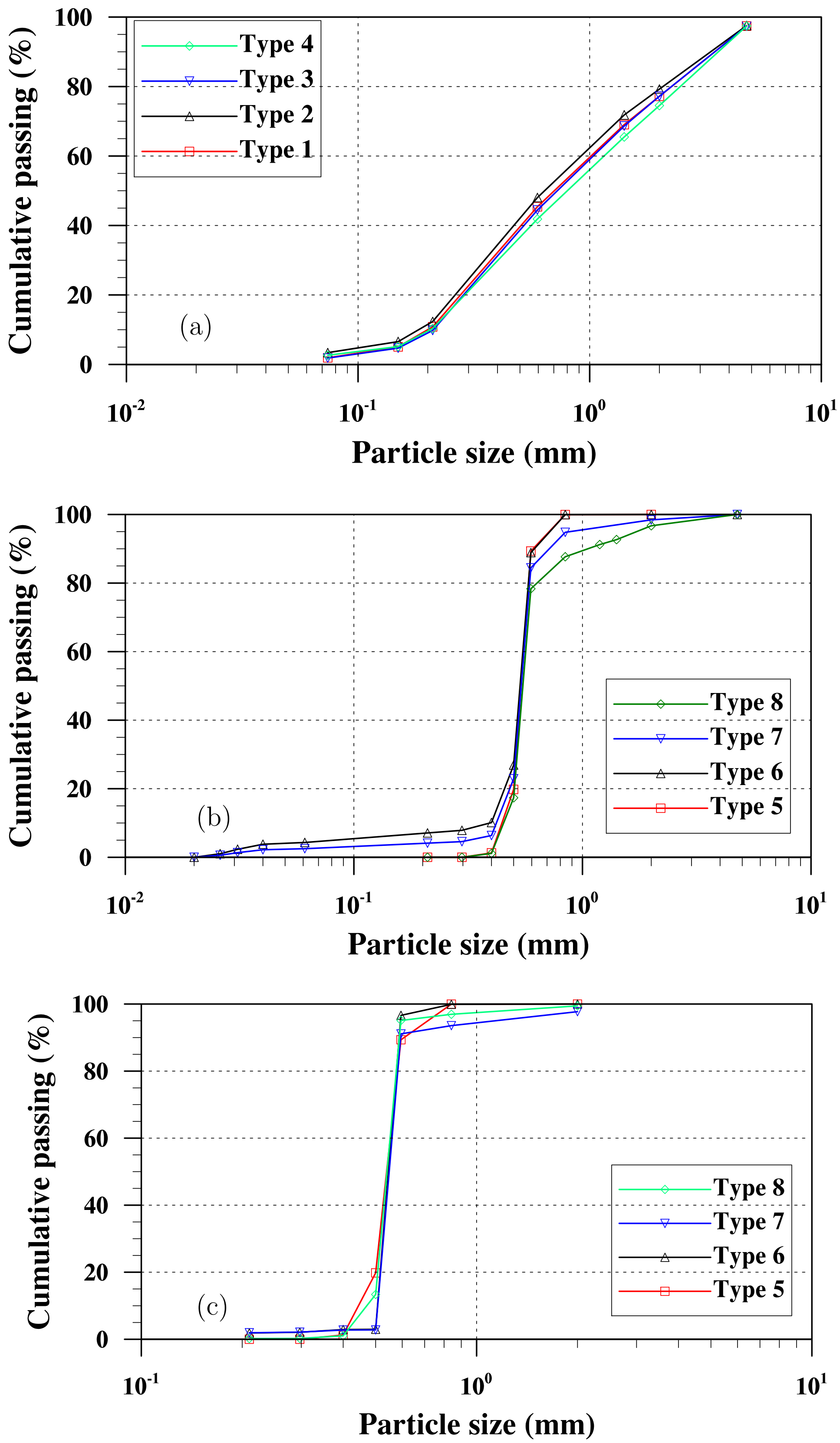

Figure 4.2: PSD for Types 1 to 8 media. (a) Mass based PSD for Types 1 to 4; (b) Volume based PSD for Types 5 to 8; (c) Mass based PSD for Types 5 to 8.

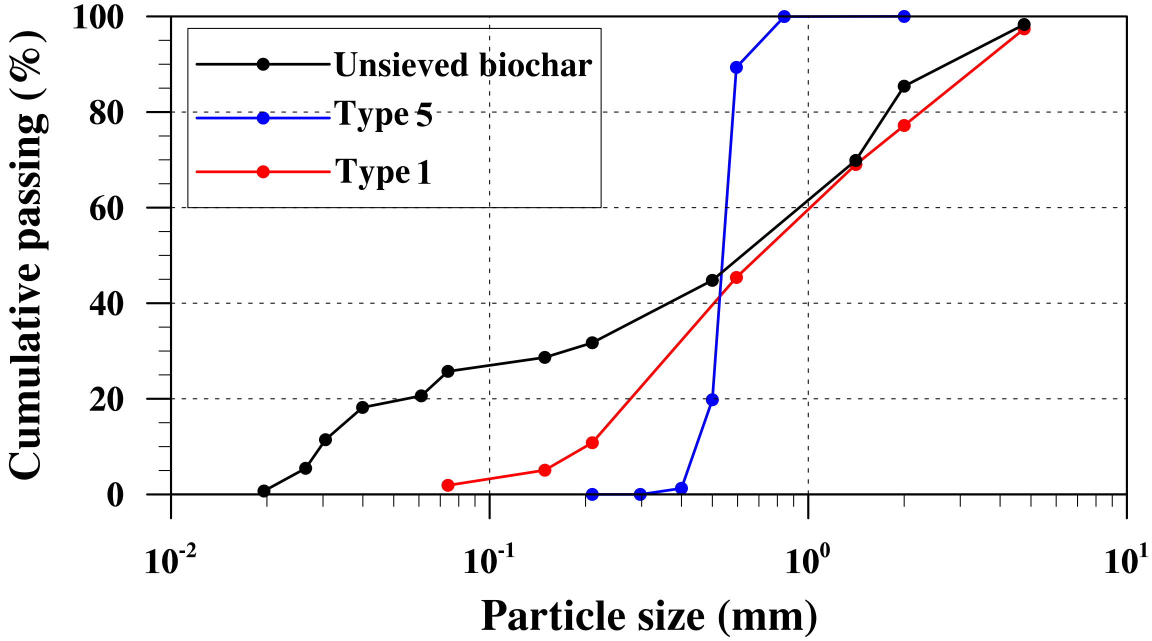

Figure 4.3: PSD for control group and unsieved biochar.

this method, with no air bubbles observed along the column wall for Type 1 and Type 5 experiments. Noticeable air bubbles can be seen around the column wall for Type 3 and Type 7 after the first 16-hr (image not shown in Figure 4.4), and the column was then submerged more deeply under de-aired DI water for another 8 hrs. Still, the air bubbles were not diminished by this process. The final gravimetric water content after 24-hr saturation time was measured to compare with the one obtained the alternative method and both results are listed in Table 4.4.

Table 4.4: Volumetric water content obtained by two saturation methods.

Type #	θ_v	
	Traditional method	Alternative method
1	0.613	0.642
3	0.457	0.616
5	0.534	0.579
7	0.426	0.619

Clearly, when it comes to samples with biochar amendment, this traditional

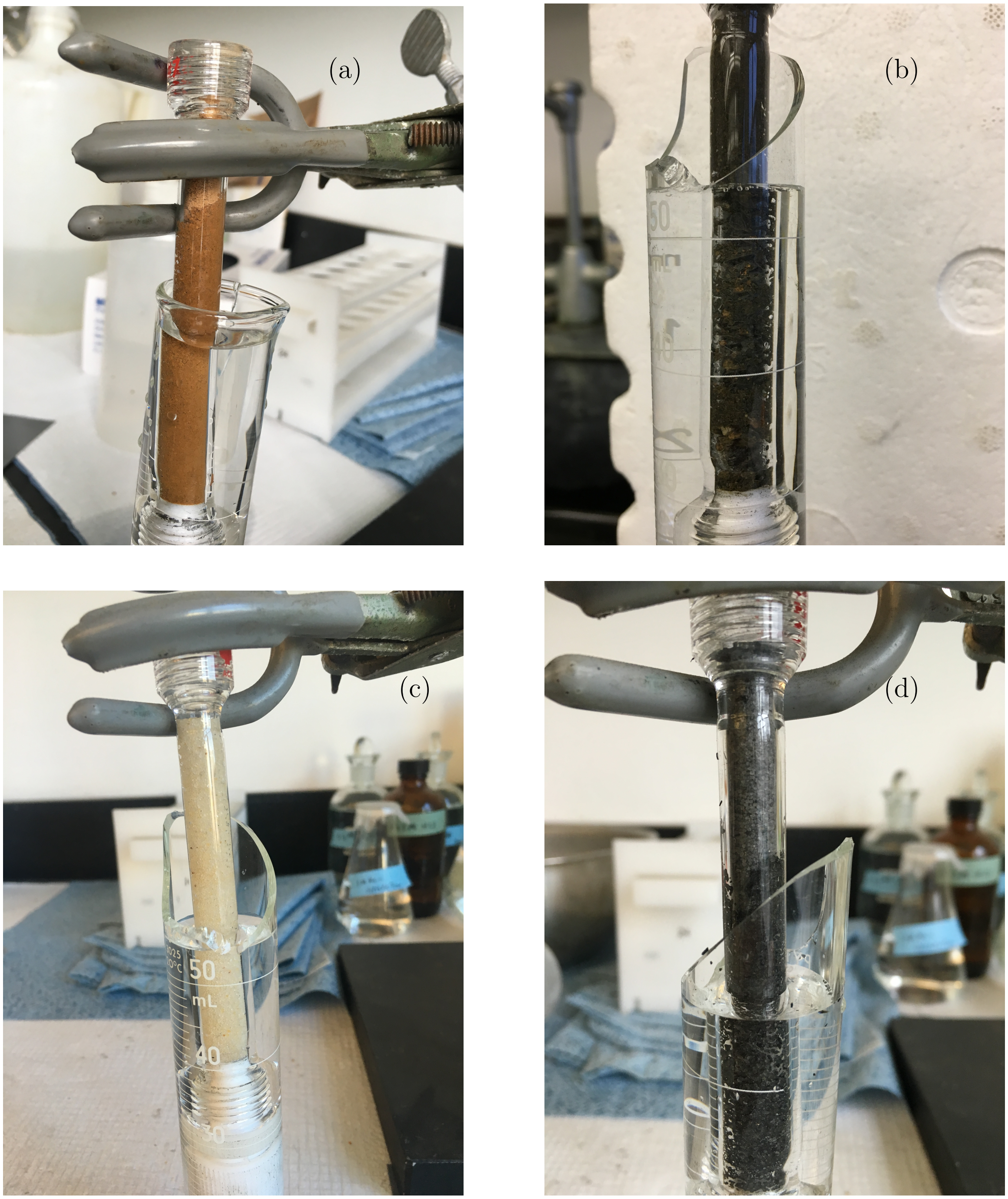

Figure 4.4: Samples using traditional saturation method. (a) Type 1 after 20-min saturation time; (b) Type 3 after 24-hr saturation time; (4)Type 5 after 16-hr saturation time; (d)Type 7 after 24-hr saturation time.

saturation method is not applicable. Biochar is irregularly shaped and when it was added into the soil, larger pores are created making it more difficult to saturate with capillary force. Based on this, it is suggested to use the alternative saturation method to achieve full saturation.

4.3.1.2 K_{sat} Measurement

The wall effect is a typical phenomenon observed in container walls caused by confined granular medium. Graton and Fraser (Graton and Fraser, 1935) found that the porosity is greater in the immediate vicinity of the container walls than in the medium body. This can be explained by nonuniform pore openings, that is, particles in contact with the container wall will not be packed as tightly as those in the body of medium, hence will have a higher porosity which causes lower resistance to flow. Franzini (Franzini, 1956) states that in order to neglect wall effects, generally the ratio of permeameter diameter to mean particle diameter should exceed about 40. d_{50} from PSD for each sediment were used to represent the mean particle diameter, and this ratio ranged between 62 to 92 (Table D.1).

Reynolds number (Re) is a dimensionless quantity that can be used to characterize flow patterns, such as laminar flow and turbulent flow. Re is defined as the ratio of inertial forces to viscous forces of a moving fluid. For flow through soils, Re can be calculated by

$$Re = \frac{Du}{\nu_k} \tag{4.1}$$

where D is the characteristic length for soils, and in this case, d_{50} is chosen to represent an average diameter of soil particles. u is velocity of the flow going through the medium, and ν_k is the coefficient of kinematic viscosity of the fluid. In this case, Re has to be under 10 to achieve laminar flow, otherwise it will start to develop turbulent flow when above 10 (Miyazaki, 2006). Since the peristaltic pump used in this study for K_{sat} measurement can be adjusted to achieve a desired flow rate, caution should be taken to avoid creating turbulent flow to the soil sample. The calculated $Re \leq 1$ in all cases during K_{sat} measurements.

Darcy's law can be written to represent K_{sat} as a proportionality constant between flux q and hydraulic head gradient, i:

$$K_{sat} = \frac{q}{i} \tag{4.2}$$

where

$$q = \frac{Q}{A} \tag{4.3}$$

and

$$i = \frac{\Delta h}{L} \tag{4.4}$$

As described in Chapter 3, three independent K_{sat} tests were performed for each sediments (except for Type 8 because of segregation in the column), and for each test the K_{sat} was determined by averaging the values at different flow rates, followed by a final averaged K_{sat} from the three separate column packings. The K_{sat} values can also be determined by taking the reciprocal of slope i vs. q (Figure 4.5). A linear trend line can be fitted into the data points, which means that Darcy's Law is valid throughout the whole dataset.

The K_{sat} results for all soil samples were tabulated in Table 4.5, along with soil bulk density and porosity. Adding biochar universally decreased soil bulk density and increased porosity, and addition of larger-size biochar lead to a higher porosity compared to addition of small and unsieved ones. However, K_{sat} did not always increase as porosity increased. The K_{sat} of the biochar-amended soils was significantly influenced by both soil and biochar particle sizes (Figure 4.6), as it is noted that distribution strongly controls the resulting pore geometry and thereby the K_{sat}. Also it has been shown that although biochar increased both intra- and inter- particles porosities (Table 4.2), the alterations of K_{sat} are largely due to changes in tortuosity of flow paths and not due to the intra-particle porosities (Lim *et al.,* 2015).

The small biochar amendment had different influences on Type 1 and 5 media. It increased K_{sat} by a factor of 1.6 for Type 1, while decreasing K_{sat} by almost 100%. Unsieved biochar resulted in the highest K_{sat} on Type 1; unexpectedly, large-size biochar increased K_{sat} less than the unsieved biochar. For Type 7 and 8, the

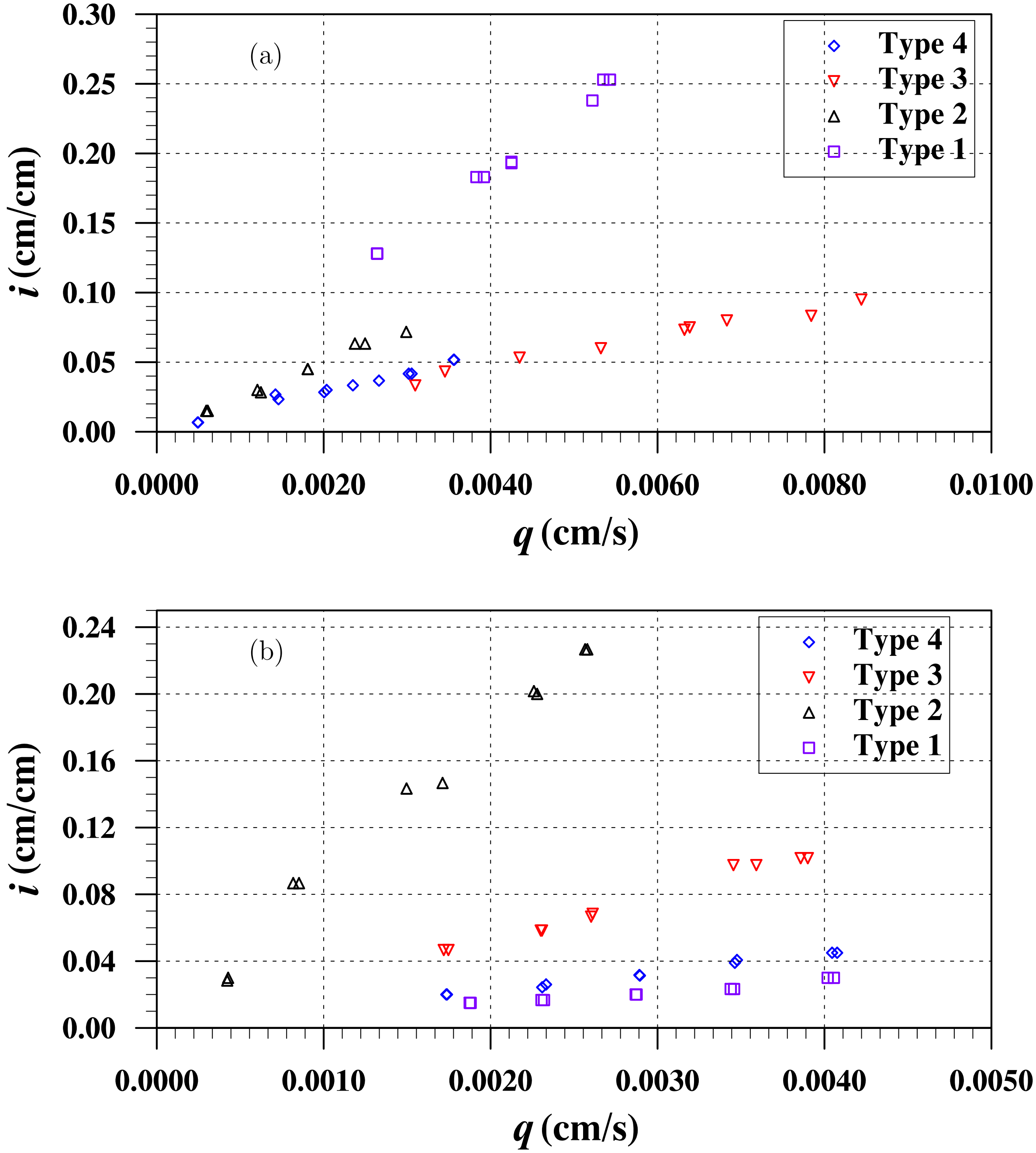

Figure 4.5: Hydraulic gradient (i) vs. Darcy's flux (q) .

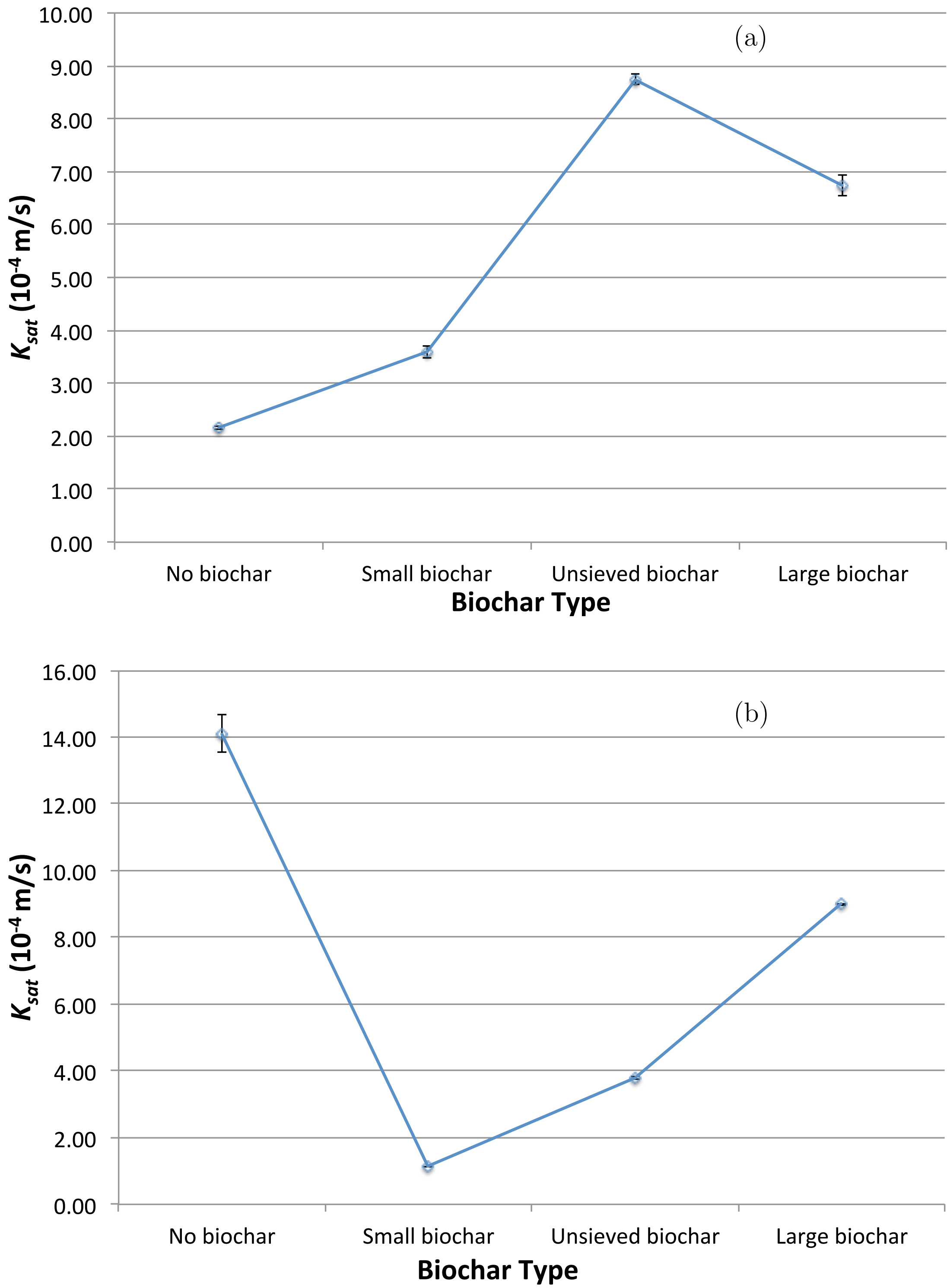

Figure 4.6: K_{sat} response with respect to biochar size. (a) Types 1 to 4; (b) Types 5 to 8. Results were calculated from three samples of Types 1 to 7, and two samples of Type 8. Error bar stands for $\pm$ 1 S.D.

Table 4.5: Dry bulk density, inter-particle porosity, and K_{sat} with associated standard deviation (S.D.) of the replicates for Types 1-8 media [a].

Type #	ρ_b		Inter-particle ϕ		K_{sat}	
	kg/m^3	S.D.	-	S.D.	m/s	S.D.
1	1515	2.307e-2	0.424	3.512e-3	2.153e-4	2.485e-6
2	1261	3.786e-3	0.451	3.786e-3	3.594e-4	1.180e-5
3	1289	1.721e-2	0.457	4.087e-3	8.750e-4	1.092e-5
4	1048	1.604e-2	0.537	1.000e-2	6.741e-4	1.914e-5
5	1736	8.627e-3	0.333	3.548e-3	1.410e-4	5.545e-5
6	1533	2.498e-2	0.332	2.909e-3	1.137e-4	1.658e-6
7	1412	1.664e-2	0.378	2.402e-2	3.798e-4	4.605e-6
8	1173	4.667e-2	0.485	1.485e-2	8.993e-4	3.627e-6

[a] Results were calculated from three samples of Types 1 to 7, and two samples of Type 8.

.

unsieved and large biochar amendment caused K_{sat} to increase compared to Type 6, however the K_{sat} was still smaller than the sample without biochar addition (Type 5). It was hypothesized that for Type 2 and 3, adding biochar created larger pores that made the flow pass easier. As for Type 4, it seems that large biochar with elongated shapes resulted in re-arrangement of the soil structure; therefore, flow rate decreased as a result of alteration of flow path. An earlier study showed a similar result; that soil amendment with biochar possessing a larger particle size had a more significant impact on K_{sat} reduction than the smaller particle size biochar (Lim *et al.,* 2015).

For Type 6 and 7, it is believed that existing fine biochar particles were placed between sand particles, thus more resistance was created that reduced the fluid flow rate. For Type 8, although large biochar produced more pores that were larger in size, K_{sat} was reduced probably due to biochar's unexpected shape impact. These results are in agreement with previous studies where K_{sat} in sandy soils decreased after biochar addition (Brockhoff *et al.,* 2010; Barnes *et al.,* 2014).

4.3.1.3 Model Predictions

As introduced in Chapter 2, six different models were tested using laboratory K_{sat} data. All measured K_{sat} for bioretention media with biochar amendment increased compared to no biochar addition. In contrast, all K_{sat} for uniform sand with biochar amendment decreased compared to the pure sand.

To be more precise in explaining the data, several parameters were defined:

$$\Delta K = \frac{K_{predicted} - K_{measured}}{K_{measured}} \tag{4.5}$$

where

ΔK is the difference between predicted (from a selected model) and measured K_{sat} for modified (with biochar) or control (without biochar) sediment.

$$\Delta K_p = \frac{K_{predicted_{modified}} - K_{predicted_{control}}}{K_{predicted_{control}}} \tag{4.6}$$

where

ΔK_p stands for the predicted difference between modified and control sediment,

$K_{predicted}$ is the predicted K_{sat} values from the models for modified or control sediment.

$$\Delta K_m = \frac{K_{measured_{modified}} - K_{measured_{control}}}{K_{measured_{control}}} \tag{4.7}$$

where

ΔK_m stands for the measured difference between modified and control sediment,

$K_{measured}$ is the measured K_{sat} from laboratory test for modified or control sediment.

The root mean square error (RMSE) for all the models was computed using two definitions for error. $E1$ represents the error between ΔK_p and ΔK_m, while E2 represents the error determined from ΔK alone.

$$E1 = \Delta K_p - \Delta K_m \tag{4.8}$$

$$E2 = \Delta K \tag{4.9}$$

4.3.1.3.1 Kozeny-Carmen (K-C)

Attempts to render K-C equation applicable to porous media have centered on determination of appropriate constants in this model. The surface area term, S_s, in Kozeny-Carmen equation, is the effective surface area of the particles exposed to the flow path, not the total surface area prior to packing (Wyllie and Gregory, 1955). Later S_s is usually estimated from the particle size distribution curve. Chapius and Légaré proposed a method to estimate S_s of a nonplastic soil from its complete grain size curve (Equation (4.10)) (Chapius and Légaré, 1992). Type 1 contains 8% clay (plastic soil), whose specific surface area should be estimated by other means (e.g. using the liquid limit obtained from Casagrande's method), but it was assumed that the plasticity will not be affected much with such a low percentage of clay; thus, we evaluated S_s following Chapius and Légaré's method.

$$S_s = \frac{6}{\rho_s} \sum_{i=1}^{n-1} \left(\frac{P_{No.\ D,i} - P_{No.\ d,i+1}}{d_{i+1}} \right) \tag{4.10}$$

where P is the percentage by weight smaller than size D ($P_{No.\ D}$) and larger than the next size d ($P_{No.\ d}$), and n stands for the total number of sieves. This method has been used in deriving S_s for nonplastic soil, yet no laboratory data were tested using this method can be used to estimate S_s of soil with biochar amendment.

According to Carmen (Carmen, 1937), the constant C, can be written in the form

$$C = k_0 \left(\frac{L_e}{L} \right)^2 \tag{4.11}$$

where k_0 is a shape factor that lies within the range 1.2 to 3.0 with 2.5 adopted for most conditions (Carmen, 1937). The determination of k_0 depends on the shape of cross-section for the channel. Carmen found that channel shapes like parallel slit will have a k_0 up to 3.0, and pipes with eccentric cores have a k_0 as low as 1.2. $(L_0/L)^2$ is the tortuosity defined as the square of the ratio of the actual average effective length of fluid flow in a porous medium, L_0, to the geometrical length of the medium in the direction of macroscopic flow, L (Wyllie and Gregory, 1955). Carmen has suggested that for all unconsolidated porous media, $(L_0/L)^2$ has a value of about 2.0. From equation 4.11, the magnitude of constant C would be between 2.4 to 6 using suggested values, and a value of 5.0 is generally employed for unconsolidated porous media (Wyllie and Gregory, 1955). Experiments have shown that the orientation of particles affects C (Sullivan and Hertel, 1942); thus, it is expected that for all the modified soils the orientated biochar particles will result in an increase in L_0 by altering water flow path, and thus lead to larger tortuosities. Practically, X-ray CT analysis can be employed to view the channel and accurately quantify the tortuosity in actual samples. For now, k_0 is assumed to be fixed for all soil types although this value certainly deviates between different sediment types. Considering that larger biochars are more angular than smaller ones (Figure 4.11), the selected constants C should follow an increasing order as biochar size increases. However, it is difficult to determine a shape factor for different biochar-amended media without further morphological information; therefore, we decided to calculate the K_{sat} in two ways: one is using the same shape factor 5.0 for Types 1 through 8; another way is to assume a constant shape factor 5.0 for control media, and use a shape factor of 6.0 for all modified types. In this way, we could see the sensitivity of K-C model by varying a shape factor.

S_s computed using from Equation (4.10) was pretty low (around 10 m^2/kg for Types 1 to 4, and 5 m^2/kg for Types 5 to 8). It is believed, though, that the biochar's rough surface should result in an increase in S_s (Mukherjee and Lal, 2014). Theoretically, it is possible to determine the external surface area exposed to flow path from X-ray CT analysis.

While measured data differ considerably from model-predicted K_{sat}, with high $E2$ values (Table 4.6), the predictions of changes in K_{sat} for bioretention media using the K-C model are encouraging: the K-C model gives comparable numbers between ΔK_p and ΔK_m for Types 2 to 4 in both cases using either shape factor (Figure 4.7 (a)). Although the magnitude of ΔK_p for Type 2 and 3 does not seem plausible compared to ΔK_m, the $E1$ values for all bioretention media are relatively small (Table 4.6). Also it can be seen that the predictions from K-C model are not significantly affected by increasing the value of shape factor, if we assume biochar amended media has a larger shape factor.

Table 4.6: RMSE of different models. $E1$ [a] represents the RMSE of ΔK_p using ΔK_m as a benchmark, and $E2$ is the RMSE for ΔK computed from Equation (4.5).

Models	Type #	$E1$	$E2$	Models	Type #	$E1$	$E2$
K-C[b]	1	-	100.91	Chapius	1	-	2.72
	2	0.48	71.83		2	*0.76*	1.03
	3	2.70	33.24		3	1.12	1.69
	4	0.35	90.24		4	3.66	7.06
	5	-	38.19		5	-	0.29
	6	0.10	88.10		6	0.36	2.85
	7	0.31	82.85		7	*1.08*	2.59
	8	*5.56*	380.82		8	*3.21*	3.28
Hazen	1	-	2.80	Shahabi	1	-	9.83
	2	*1.01*	0.51		2	0.49	6.62
	3	1.26	1.62		3	2.35	3.57
	4	0.52	3.42		4	0.38	11.05
	5	-	1.24		5	-	0.59
	6	0.27	8.28		6	0.82	3.55
	7	0.58	5.72		7	*1.45*	1.64
	8	*0.41*	2.48		8	*4.84*	2.50
NAVFAC	1	-	3.08	Fair-Hatch[c]	1	-	15.73
	2	0.65	1.49		2	0.45	11.2
	3	0.76	3.85		3	2.67	4.74
	4	19.2	28.19		4	0.32	0.38
	5	-	0.07		5	-	0.03
	6	0.18	2.03		6	0.14	1.71
	7	*1.11*	3.80		7	*0.42*	1.53
	8	*6.36*	9.22		8	*6.04*	9.28

[a] Italicized $E1$ indicates a wrong direction of prediction in K_{sat}.
[b] $E1$ and $E2$ were calculated using shape factor 5 for all Types.
[c] $E1$ and $E2$ were calculated using shape factor 6.1 and 6.0 for Types 1 to 4, and Types 5 to 8, respectively.

.

For Type 6 and 7, this model predicts a decrease in K_{sat}, which is what we measured in laboratory, no matter which shape factor was employed (Figure 4.8 (a)). For Type 8, the void ratio calculated using only the inter-particle porosity was greatly

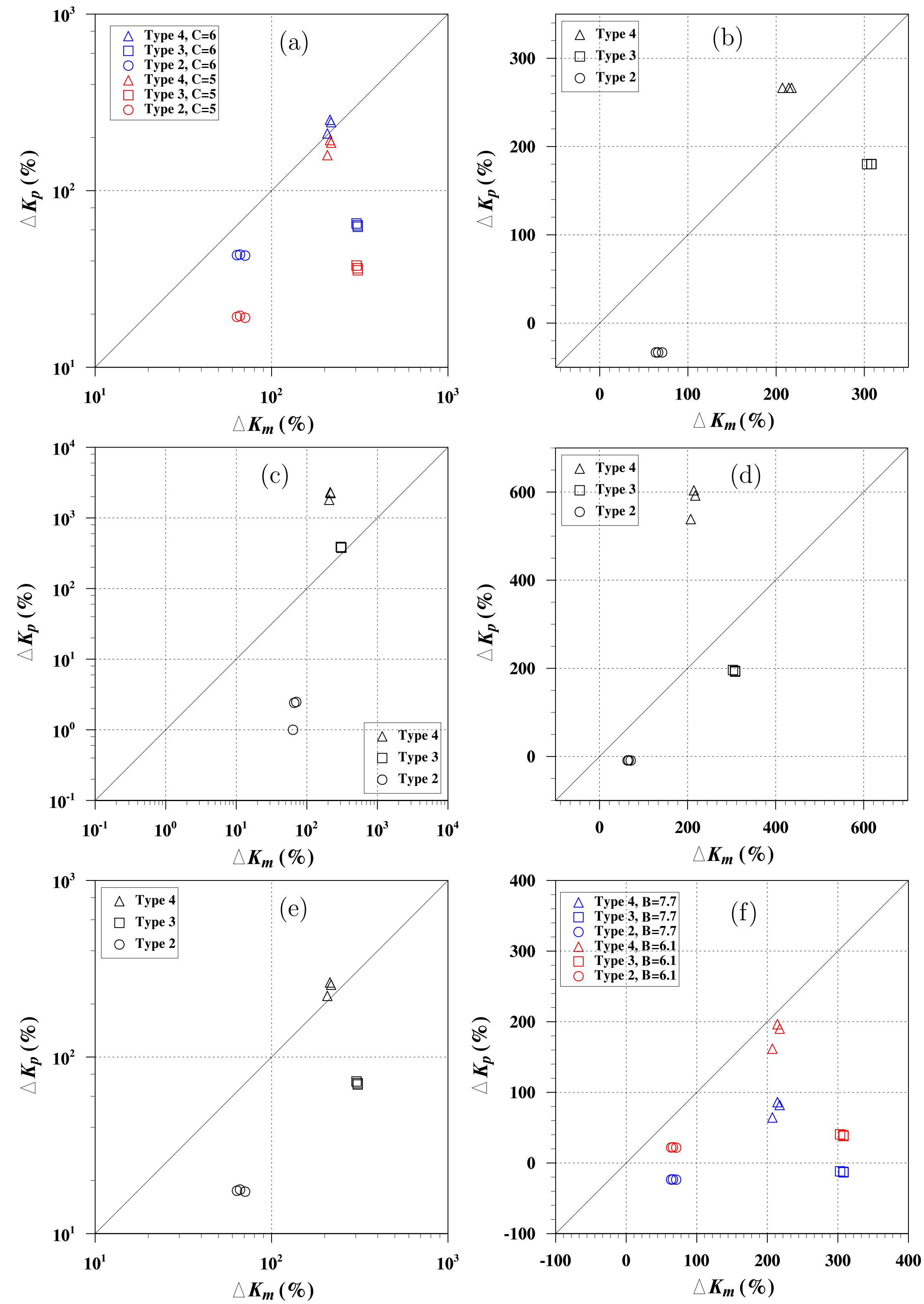

Figure 4.7: Comparison between predicted and measured changes in K_{sat} for Types 2 to 4. (a) Kozeny-Carmen (b) Hazen (c) NAVFAC (d) Chapius (e) Shahabi (f) Fair-Hatch

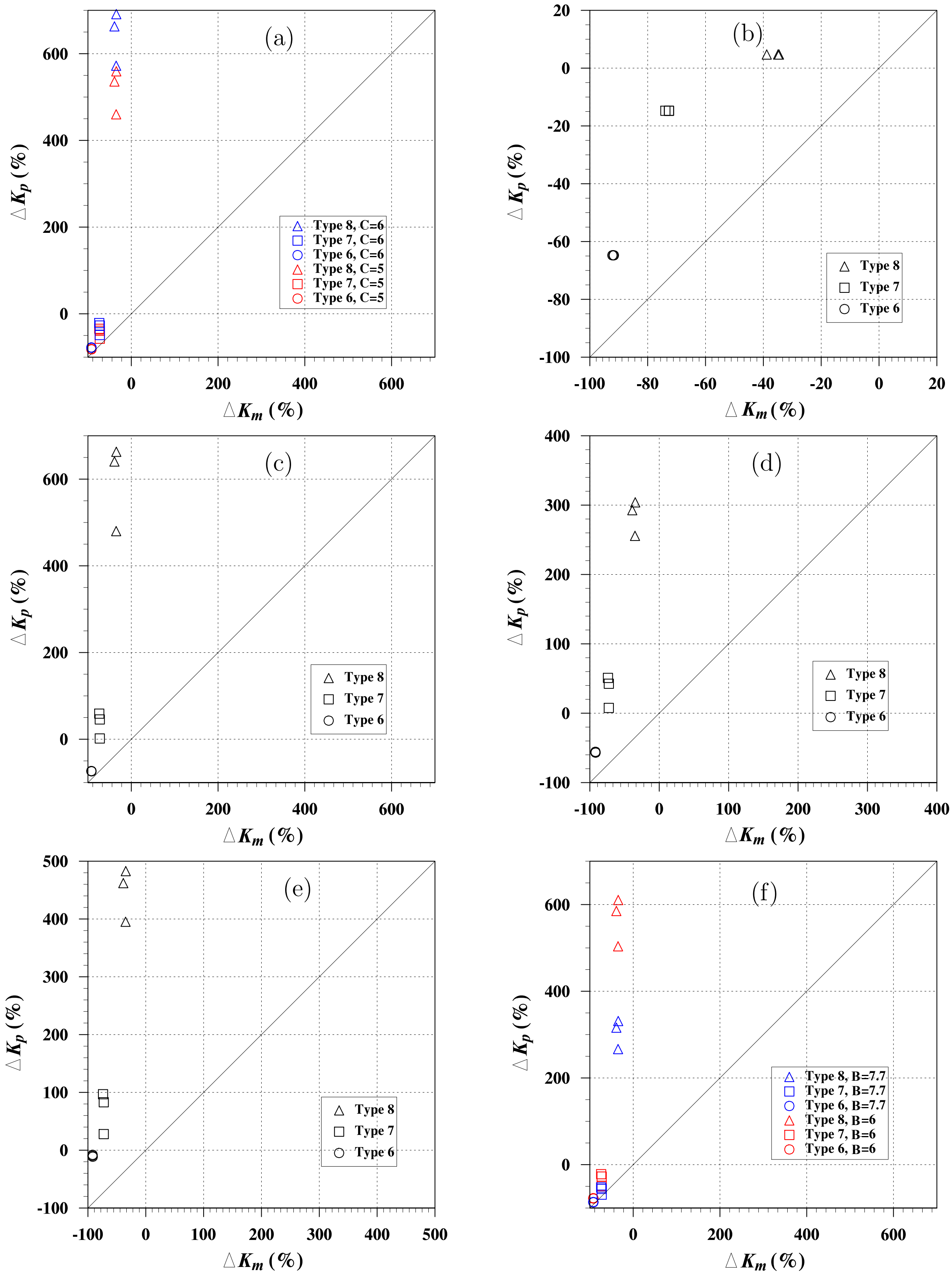

Figure 4.8: Comparison between predicted and measured changes in K_{sat} for Types 6 to 8. (a) Kozeny-Carmen (b) Hazen (c) NAVFAC (d) Chapius (e) Shahabi (f) Fair-Hatch

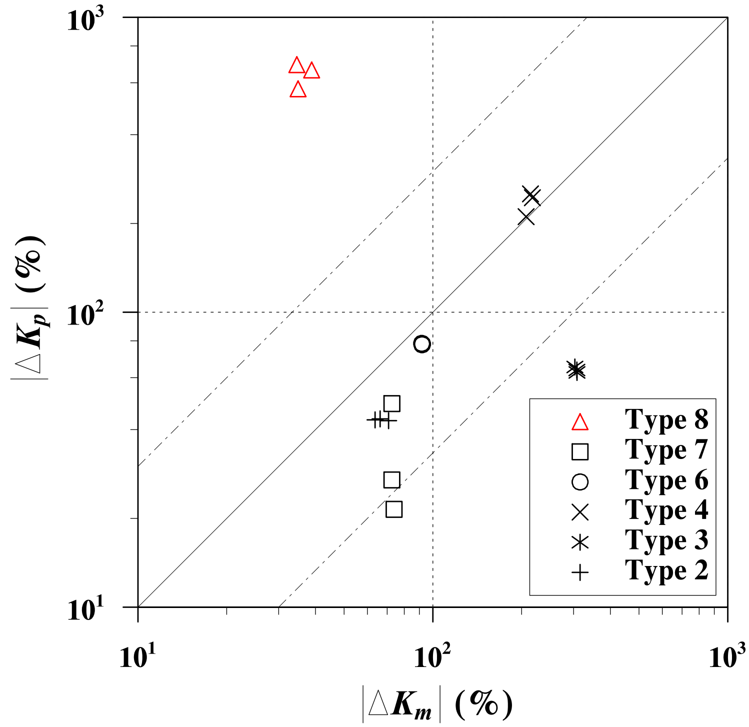

Figure 4.9: Kozeny Carmen for Types 2 to 4, and 6 to 8. ΔK_p and ΔK_m are expressed as absolute values; and the outliers for Type 8 indicates an incorrect prediction of change in K_{sat}. Diagonal (equivalent) line represents 1:1 values, and area between the other two lines represent data that are within a factor of 3 of actual values.

increased by adding larger biochar (88%), and K_{sat} is predominantly controlled by void ratio in the K-C equation (Equation (2.2)). Thus K_{sat} is predicted to be larger than that for Type 5, while actual K_{sat} were less than that for Type 5 media. It is hypothesized that large biochar particles that are shaped more elongated might cause unexpected changes to the sediment structure; also, porous medium in Type 8 column appeared non-homogeneous and segregated, with distinct layers of high and low concentrations of large biochar. Similar segregation was not observed for any other packing. Thus, the flow paths in Type 8 media were likely much more nonuniform that predicted by the K-C model, resulting in significant disparity between model predictions and measured data.

Figure 4.9 shows that overall, K-C model is capable of predicting biochar's effect on K_{sat} for all media except Type 8. The ΔK_p and ΔK_m are expressed as absolute values because some of the numbers are negative for Types 6 to 8; and the outliers for Type 8 indicates an incorrect prediction of change in K_{sat}.

4.3.1.3.2 Hazen

Particle size distribution for each sediment sample was plotted to obtain d_{10} that was used in Hazen equation (Equation (2.3)). As mentioned before, the temperature did not change much during K_{sat} measurements, so a dimensionless constant was used in Hazen equation. Hazen equation can be applied when $C_u < 5$, and this condition was satisfied by Types 3 to 8. Calculations showed that the predicted K_{sat} of Type 1 is as large as almost 4 times of laboratory K_{sat}, the predicted K_{sat} of Type 5 is approximately 2 times of measured K_{sat}, and for Type 2, 3 and 4, the model gives K_{sat} values that are all within a factor of 5 of the measured K_{sat} (Table E.1).

Small biochars reduced the d_{10} for Type 2, and unsieved and large biochars increased d_{10} for Types 3 to 4 compared to Type 1. Consequently, the Hazen equation (Equation (2.3)) provided ΔK_p with a correct direction for Types 3 and 4 but gave an incorrect prediction for Type 2 (Figure 4.7 (b)). Similarly, for Types 6 and 7, both of their d_{10} were smaller than Type 5; thus, the predicted K_{sat} for Types 6 and 7 will be smaller than predicted K_{sat} for Type 5, which is in agreement with the ΔK_m (Figure 4.8 (b)).

This model solely depends on the particles size without considering particle geometry. Adding biochars increased the d_{10} for Type 8, however, the model ignores the fact that being smooth uniform sand, tortuosity and surface resistance may increase by a huge factor with amended biochar compared to Type 5, and the change in particle surface and structure can result in a dramatic decrease in K_{sat}. Therefore, although Hazen's equation correctly predict the direction of change in K_{sat} for Types 3, 4, 6, and 7, it ignores the particle structural impacts of biochar amendment.

4.3.1.3.3 NAVFAC

Among all the sediment samples, none of the them satisfies the three conditions introduced in Chapter 2 for the NAVFAC model. Surprisingly, the predicted absolute K_{sat} values for eight samples seemed reasonable as $E2$ values for all media are relatively small (Table 4.6). Table E.1 lists the percent difference between predicted and measured K_{sat}.

NAVFAC correctly predicted the direction of change in K_{sat} for all bioretention media (Figure 4.7 (c)), and Type 6 (Figure 4.8 (c)). For Type 7 and 8, d_{10} and void ratio increased at the same time, thus the model gives a higher K_{sat} in both cases, while actual K_{sat} decreased with biochar addition to this sand. It is likely that unsieved and large biochar with irregular shapes created unexpected structure variations to the sample, which contributed to a decrease in measured K_{sat} (Figure 4.8 (c)). The $E1$ values are relatively low for Type 2 and 6, meaning that to some extents, NAVFAC can be used to predict the K_{sat} changes with small biochar additions for bioretention media and uniform sand. Considering an increase in surface roughness and tortuosity as a result of amended biochar. The NAVFAC model might be modified to include the shape and surface resistance effects to better predict changes in K_{sat} with biochar addition.

4.3.1.3.4 Chapius

As introduced in Chapter 2, Chapius stated that this model may be used for any natural non-plastic soil including silty soils with $0.003 \leq d_{10} \leq 3$ mm and $0.3 \leq e \leq 1$. Based on the calculation of percent difference between predicted and measured K_{sat}, Chapius model seems to give reasonable absolute K_{sat} values for Types 1, 2, 3, and 5 (Table E.1), even though none of these are natural soils.

As shown in Figure 4.7 (d), Chapius was able to produce ΔK_p in the same direction as ΔK_m for Types 3, 4 and 6. Small biochar lowered d_{10} for Type 2 compared to Type 1. Although the void ratio increased, this change was not significant enough to increase K_{sat} (Equation 2.8); thus, the model yields a smaller K_{sat} for Type 2 than

Type 1. While the laboratory K_{sat} showed that small and unsieved biochar lead to increases in K_{sat}, the model is unable to provide a correct prediction of K_{sat} change for Type 2.

Adding irregularly shaped biochars will make the soil geometry change inside the column. This model is only dependent on d_{10} and e without considering the particles shapes or packing factors. Therefore, for Types 7 to 8, the prediction gave an opposite directions of ΔK_p compared to ΔK_m. As an empirical model, Chapius provides a poor prediction in K_{sat} since it does not incorporate soil structure variations.

4.3.1.3.5 Shahabi

As mentioned previously in Chapter 2, in order to use Shahabi equation (Equation (2.9)), four conditions must be verified. Although only Type 5 satisfied all the requirements, application of this model to Type 2, 3, and Types 5 to 8 all yielded reasonable predictions of K_{sat} (Table E.1).

For Types 2, 3, 4, and 6, Shahabi produced correct predictions of ΔK_p in terms of direction (Figure 4.7 (e), Figure 4.8 (e)), with rather low $E1$ values (Table 4.6), but it did not work for Type 7 and Type 8. K_{sat} in this model is proportional to C_u, d_{10}, and void ratio, e. C_u and d_{10} for Types 6 to 8 differ by less than 15% from Type 5, whereas e for Type 6 is smaller than Type 5 and e of Type 7 and 8 are larger than Type 5. The dominant term $(e^{3+x})/(1+e)$ contributed to a huge increase in predicted K_{sat} values (Equation (2.9)). Accordingly, Shahabi equation predicted changes to K_{sat} in the wrong direction for Type 7 and 8. Again, these results can be explained by the fact that this model ignores surface roughness and thus the increase in resistance caused by biochar particle. Therefore, the model might be modified to include particle roughness..

4.3.1.3.6 Fair-Hatch

In the Fair-Hatch equation, the dimensionless packing factor A was chosen to be 5.0 and the particle shape factor B was selected by comparing biochar particles used in this study to those shown in Figure 4.10 (Fair and Hatch, 1933). In that figure from 1 to 4 are: angular sand with a shape factor 7.7, sharp sand with a shape factor 7.4, worn sand with a shape factor 6.4, and rounded sand with a shape factor 6.1, respectively. Also as described in Fair and Hatch's study, shape factor of spherical sand is 6.0.

Type 1 consists of mostly concrete sand which is rounded, so a shape factor of 6.1 was used; 30/40 accusand is highly spherical so that a shape factor of 6.0 was selected. Particles images from morphology measurements (Figure 4.11) showed that a larger biochar particle is more angular than a smaller biochar particle; however, it is difficult to determine the exact value of the shape factor for different sediments without further morphological information; therefore, the ΔK_p was calculated in two ways: one is using the same shape factor 6.1 for Types 1 through 4, and 6.0 for Types 6 through 8, while in the second procedure a value of 7.7 was used for all types modified with biochar (Types 2 to 4, and 6 to 8), while retaining 6.1 and 6.0 for Type 1 and 5, respectively. By doing this we could see how sensitively the model responds to a change in the shape factor.

Additionally, the term F in Fair-Hatch (Equation (2.10)) was developed to represent the percent by weight of the sample between two successive sieve sizes. As for Types 5 to 8, the PSDs were plotted based on the volume instead of the mass of the sediment, and F is accordingly revised by calculating the percent by volume of the sample between two successive sieve sizes. For Types 2 to 4, since the parameters used in the models were determined by PSDs plotted based on the mass of the sediment, the F is thereby retained as mass based form.

From Figure 4.7(f), it is interesting to see that using the same shape factor for all bioretention media, the model was able to provide the same direction of change in K_{sat} as measured K_{sat}. Contradictorily, based on the assumption that biochars are angular and using the shape factor 7.7 derived from Fair-Hatch's study for media that included biochar, this model produced an incorrect change in direction of K_{sat} for Type 2 and 3 media. Additionally, Fair-Hatch model predicted the direction of the K_{sat} influence accurately for Type 6 and 7 regardless the shape factor variations, while

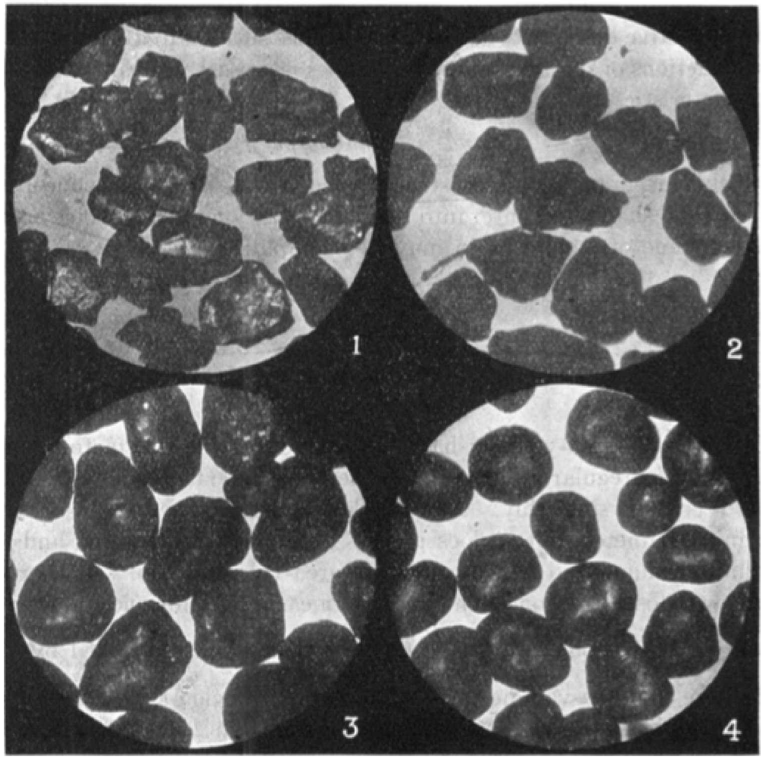

Figure 4.10: Shape of filter sands. From 1 to 4 are: angular sand, sharp sand, worn sand, and rounded sand (Fair and Hatch, 1933). (Reprinted from Journal AWWA, Vol. 25, by permission. Copyright ©1933 American Water Works Association.)

the prediction was in the incorrect direction for Type 8 (Figure 4.8 (f)). As has been illustrated before, for Type 8 an opposite ΔK_p compared to ΔK_m might be attributed to segregation in the column or an unexpected structural or surface roughness change in the sediment.

Fair-Hatch equation worked very well for pure uniform sand, as there was only a 2% difference between measured and predicted K_{sat} of Type 5 (E.1). Speaking of Type 1 sediment, this model yields a 15 times larger K_{sat} than measured data. The reason can be attributed to inadequate information of packing factor A and shape factor B. This model was initially developed by Fair and Hatch for filtration system that consisted primarily of sand rather than engineered bioretension system that has small particles with clay and sawdust in it. Thus, the values for parameters A and B might vary with respect to sediment type.

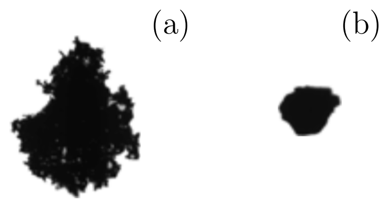

Figure 4.11: Biochar images from morphology measurement. (a) Particle with a CE diameter of 585.83 μm; (b) Particle with a CE diameter of 226.25 μm, where CE diameter stands for circle equivalent diameter, which is the diameter of a circle with the same area as the 2D image of the particle.

Looking at Type 2, 3, 4, 6 and 7, Fair-Hatch predicts the correct directional change in ΔK_p (Figure 4.7 (f) and Figure 4.8 (f)). Compared to Type 5, while the measured and predicted K_{sat} for this sample are almost identical, the predicted K_{sat} of Type 8 increased as large biochar were added, while measured K_{sat} decreased. Thus, the Fair-Hatch equation worked well for the bioretention media amended with biochar using a shape factor of 6.1, but poorly when large biochar was added to the uniform sand.

4.3.2 Field Infiltrometer Test

Zimmermann *et al.* (2006) states that the in-situ measurements of K_{sat} in the unsaturated zone results in air bubbles entrapped in the soil due to the advancing wetting front. Hence, the water content of a "field-saturated" soil is usually lower than at complete or true saturation. This means field measurements will underestimate true K_{sat}.

The initial and final soil water content (θ_i and θ_f) were measured by taking core samples before and after the experiment. Parameters θ_s, α and n where fitted while θ_r and l are assumed to be constant. After iteration of the results, the outcomes for predicted saturated water content, α, n and K_{sat} were provided, along with standard errors and 95% confidence interval. As initially our focus is on Type 1 and 3, the input data and outcome of DISC for these two types are listed in Table 4.7.

For Type 1, laboratory K_{sat} is 6 times higher than hydraulic conductivity data

Table 4.7: Results from DISC[a].

Type No.	Input parameters					Hydraulic Conductivity (cm/s)	
	θ_i	θ_f	θ_s	α	n	K	S.D.
1	0.22	0.36	0.41	0.124	2.28	3.486e-03	5.000e-05
3	0.24	0.44	0.41	0.124	2.28	5.284e-03	7.000e-05

[a] Results are averaged by two core samples.

obtained from DISC and 26 times higher for Type 3. This can be explained by entrapped air in the field bioretention media. Thus, the measured hydraulic conductivities are not true K_{sat}, it is the conductivity corresponding to the water content provided. Even though these data underestimated K_{sat} and they can not represent the intrinsic properties of the field soils, they are helpful in knowing the performance of the stormwater remediation media under realistic conditions.

Chapter 5

CONCLUSION AND FUTURE WORKS

Laboratory K_{sat} were measured for two control sediments (Type 1 and 5), and six sediments modified with biochar (Types 2 to 4, and Types 6 to 8). The incorporation of biochar into bioretention media (Type 1) and sand (Type 5) revealed a decrease in soil bulk density accompanied by an increase in total porosity for all modified soils.

Increase in porosity was likely attributed to two theoretical flow pathways; one is the interstitial space within the biochar-soil matrix created by biochar amendment (inter-particle pores) and the second internal pores within the bichar (intra-particle pores). Since it is likely that the second pathway has greater tortuosity, as well as lack of complete connectivity, inter-particle porosity likely has a dominant effect on K_{sat}. (Brewer *et al.,* 2014). Depending on the soil type and particle size of biochar, inter-particle porosity may or may not be altered when biochar is added to the sediment. For bioretention media, small and unsieved biochar showed similar increases in inter-particle porosity, whereas for uniform sand, small biochar had nearly no impact on the inter-particle porosity.

An increases in porosity was not always concomitant with in an increase in K_{sat}, and the changes in physical soil properties are not sufficient to explain the hydrologic changes. In samples where inter-particle porosity increased but K_{sat} decreased, the biochar grains likely created tortuous interstitial space between the sample matrix to decrease K_{sat} (Barnes *et al.,* 2014). Another mechanism leading to K_{sat} reduction could be related to physical change of the media in the column such as swelling, although we only observed visible segregation for Type 8 sediment. The location of biochar within the soil also affects K_{sat}. Previous hydraulic conductivity tests showed that uniformly mixed sample with biochar had a 67% higher hydraulic conductivity compared to the samples which biochar was placed in the center of it (Zhang *et al.,* 2016). Therefore, even though porosity is often increased when biochar is amended to sediments, as Reddi *et al.* (2015) pointed out, some fine biochar particles may clog conductive pores in the soil matrix.

Overall, the six models tested in this study showed reasonable predictions for the effect of biochar on K_{sat} in bioretention media, except for Type 2 sediment where Hazen and Chapius models predicted decreases in K_{sat} while it actually increased. All of the models were able to predict the direction of the K_{sat} changes for Type 6 but not Type 8 media, while Kozeny-Carmen and Hazen models successfully predicted the change in direction of K_{sat} for Type 7 media. In the Kozeny-Carmen model, variations in the shape factor will not cause a significant change in the prediction for sediments modeled; however, the Fair-Hatch model is very sensitive to the shape factor for Types 2 to 4 media, in which case causing predicted K_{sat} to increase or decrease depending on the value of the shape factor.

It has been widely recognized that saturated hydraulic conductivity is influenced by the particle size distribution of biochar, its application rate, and soil texture. Based on the observations from this study, internal structure alteration of sediments amended with biochar may also affect K_{sat} which resulted in the unusual behavior for Type 8 media of K_{sat}. To better understand the mechanism by which biochar alters K_{sat} particularly in sandy soils, it is necessary to "see" the internal structure of soil-biochar sample using tools such as X-ray computed tomography. Morphology tests of biochar particles show that biochar particles have different shapes that vary with particle size. Thus, biochar amendments of different particle sizes will likely alter pore geometries differently. This hypothesis may only be tested using X-ray computed tomography.

For those predictive models investigated in this study, there are a number of possible modifications that could be made to further improve the models. First of all, the specific surface area term in Kozeny-Carmen equation could be modeled and computed by X-ray CT analysis in order to improve the performance of this model. Second, the packing factor in Fair-Hatch equation might be altered depending on biochar amendment, which can also possibly be tested by X-ray CT analysis. Shape factors may be included and/or modified in these models to improve model predictions.

REFERENCES

Ajayi, A.E., D. Holthusen, and R. Horn. 2016. “Changes in microstructural behaviour and hydraulic functions of biochar amended soils”. Soil & Tillage Research. 155: 166-175.

Allan, J. D., Castillo, Maria, M., 2007. “Stream Ecology: Structure and function of running waters (2nd ed.).” Dordrecht, The Netherlands: Springer

ASTM International, 2013. D3766 08, “Standard Terminology Relating to Catalysts and Catalysis.” pp.1.

ASTM International, 2014. C136/C136M 14, “Standard Test Method for Sieve Analysis of Fine and Coarse Aggregates.” pp.2-3.

ASTM International, 2007. D4972 01, “Standard Test Method for pH of Soils.” pp.1-2.

ASTM International, 2007. D422 63, “Standard Test Method for Particle-Size Analysis of Soils.” pp.5.

ASTM International, 2013. D3766 08, “Standard Terminology Relating to Catalysts and Catalysis.” pp.1.

Bachmann, J., Ellies, A., Hartge, K., 2000. “Development and application of a new sessile drop contact angle method to assess soil water repellency.” J. Hydrol. 231232:6675.

Barnes, R.T., Gallagher, M.E., Masiello, C.A., Liu, Z., Dugan, B., 2014. “Biochar-Induced Changes in Soil Hydraulic Conductivity and Dissolved Nutrient Fluxes Constrained by Laboratory Experiments.” PLoS ONE 9(9): e108340.

Bear, J., 2007. “Hydraulics of groundwater.” Mineola, N.Y: Dover Publications.

Beck, D. A., Johnson, G. R., and Spolek, G. A.2011. “Amending greenroof soil with biochar to affect runoff water quantity and quality.” Environmental pollution, 159(8-9), 2111-2118.

Bisdom, E.B.A., Dekker, L.W., Schoute, J.F.Th., 1993. “Water repellency of sieve fractions from sandy soils and relationships with organic material and soil structure.” Geoderma, 56, 105 118.

Brewer, C.E., Chuang, V.J., Masiello, C.A., Gonnermann, H., Gao, X., Dugan, B., Driver, L.E., Panzacchi, P., Zygourakis, K., Davies, C.A., 2014. “New approaches to measuring biochar density and porosity.” Biomass and Bioenergy. 66, 176e185.

Brockhoff, S.R., Christians, N.E., Killorn, R.J., Horton, R., Davis, D.D., 2010. “Physical and mineral-nutrition properties of sand-based turfgrass root zones amended with biochar.” Agron. J. 102, 16271631.

Brown, R., 2009. “Biochar production technology, in Lehmann, J & Joseph, S. Biochar for environmental management: science and technology.” Earthscan, United Kingdom: 12746.

Bridgwater, A.V., Meier, D., Radlein, D., 1999. “An overview of fast pyrolysis of biomass.” Organic Geochemistry, 30 (12), 1479-1493. doi: 10.1016/S0146- 6380(99)00120-5

Carman, P.C., 1937. Trans. Inst. Chem. Engrs. (London),15,160.

Carrier III, W.D., 2003. “Goodbye, Hazen; Hello, Kozeny-Carman.” Journal of Geotechnical and Geoenvi-ronmental Engineering Vol. 129, No. 11.

Chapuis, R.P., and Legare, P.P. 1992. “A simple method for deter- mining the surface area of fine aggregates and fillers in bitumi- nous mixtures. In Effects of aggregates and mineral fillers on asphalt mixture performance.” American Society for Testing and Materials, ASTM STP Vol. 1147, pp. 177186.

Chapius, R.P., 2012. “Predicting the saturated hydraulic conductivity of soils: a review.” Bull Eng Geol Environ. 71:401434.

Chapius, R.P., 2004. “Predicting the saturated hydraulic conductivity of sand and gravel using effective diamter and void ratio.” Can. Geotech. J. 41 :787-795.

Cheng, C.H., Lehmann, J., Engelhard, M.H., 2008. “Natural oxidation of black carbon in soils: Changes in molecular form and surface charge along a climosequence.” Geochimica et Cosmochimica Acta 72, 15981610.

De Gryze, S., Six, J., Brits, C., Merckx, R., 2005. “A quantication of short-term macroaggregate dynamics: inuences of wheat residue input and texture.” Soil Bio. Biochem. 37, 55-66.

Doerr S.H., 1998. “On standardizing the water drop penetration time and the molarity of an ethanol droplet techniques to classify soil hydrophobicity: A case study using medium textured soils.” Earth Surf. Processes Landforms, 23, 663 668.

Downie, A., Crosky,A., Munroe. P.. 2009. “Physical properties of biochar. ” pp. 13-32. In J. Lehmann and S. Joseph (eds.) Biochar for environmental management: Science and technology. Earthscan, London.

Franzini, J.B., 1956. “Permeable Wall Effect.” Transactions, American Gepphisical Union, Vol 37, No6.

Fair, G.M., Hatch, L.P., Hudso, H.E., and Jr. 1933. “FUNDAMENTAL FACTORS GOVERNING THE STREAMLINE FLOW OF WATER THROUGH SAND [with DISCUSSION].” Journal (American Water Works Association), Vol. 25, No. 11 (NOVEMBER, 1933), pp. 1551-1565

Ghodrati, M., Sims, J., Vasilas, B., 1995. “Evaluation of fly ash as a soil amendment for the Atlantic Coastal Plain: I. Soil hydraulic properties and elemental leaching.” Water, Air, Soil Pollut. 81, 349361.

Giesche, H.,2006. “Mercury porosimetry: a general (practical) overview.” Part Syst Charact;23(1):9e19.

Glaser B., Lehmann J., Zech, W., 2002. “Ameliorating physical and chemical properties of highly weathered soils in the tropics with charcoal - a review.” Biology and Fertility of Soils 35: 219230.

Graton, L.C., Fraser, H.J., 1935. “Systematic packing of spheres with particular relation of porosity to permeability”. J. Geol., 42, 785-909.

Šimůnek. J., van Genuchten M. Th., 2000. “The DISC Computer Software for Analyzing Tension Disc Infiltrometer Data by Parameter Estimation.” Research Report No. 145.

Hale, S.E., Hanle, K., Lehmann, J., Zimmerman, A.R., Cornelissen, G., 2011. “Effects of chemical, biological, and physical aging as well as soil addition on the sorption of pyrene to activated carbon and biochar.” Environmental Science & Technology 45, 1044510453.

Hardie, M., Brent C., Sally B., Garth O., and Dugald C., 2014. "Does biochar influence soil physical properties and soil water availability?" Plant and Soil : An International Journal on Plant-Soil Relationships. 376 (1-2): 347-361.

Hazen, A., 1892. "Some physical properties of sand and gravel, with special reference to their use in filtration." In Massachusetts State Board of Health, 24th Annual Report, Boston, Mass., pp. 539 556.

Herath, H.M.S.K., Camps-Arbestain, M., Hedley, M., 2013. "Effect of biochar on soil physical properties in two contrasting soils: an Alfisol and an Andisol." Geoderma. 209210, 188197.

JuryW.A.Horton, R., 2004. "Soil Physics". John Wiley & Sons, Inc. New Jersey.

Kalra, Y., Maynard, D., 1991. "Methods manual for forest soil and plant analysis." Edmonton, Alberta.

Kameyama, K., Miyamoto, T., Shiono, T., Shinogi, Y., 2012. "Influence of sugarcane bagasse-derived biochar application on nitrate leaching in calcaric dark red soil." J. Environ. Qual. 41, 11311137.

Klute. A., 1965."Methods of Soil Analysis." Part 1, 13, pg 210.

Laird, D.A., Brown, R.C., Amonette, J.e., Lehmann, J., 2009b. "Review of the pyrolysis platform for coproducing bio-oil and biochar." Biofuels Bioproducts & Biorefining, 3(5), pp.547562.

Laird, D.A., Rogovska, N.P., Garcia-Perez, M., Collins, H.P., Streubel, J.D., Smith, M., 2009a. "Pyrolysis and Biochar-Opportunities for Distributed Production and Soil Quality Enhancement." Sustainable Alternative Fuel Feedstock Opportunities, Challenges and Roadmaps for Six U.S. Regions, Chap 16, pg 257.

Laird, D.A., Fleming, P., Davis, D.D., Horton, R., Wang, B., Karlen, D.L., 2010. "Impact of biochar amendments on the quality of a typical Midwestern agricultural soil." Geoderma 158, 443449.

Leelamanie D. A. L., Karube J., Yoshida A., 2008. "Characterizing water repellency indices: Contact angle and water drop penetration time of hydrophobized sand." Soil Science and Plant Nutrition 54, 179187.

Leelamanie D. A. L., Karube J., Yoshida A., 2010. "Clay effects on the contact angle and water drop penetration time of model soils." Soil Science and Plant Nutrition 56, 371375.

Lehmann J., Gaunt J., Rondon, M., 2006. "Bio-char sequestration in terrestrial ecosystems - A review." Mitigation and Adaptation Strategies for Global Change 11: 403427.

Lehmann, J., da Silva Jr, J.P., Steiner, C., Nehls, T., Zech, W., Glaser, B., 2003. "Nutrient availability and leaching in an archaeological Anthrosol and a Ferralsol of the Central Amazon basin: fertilizer, manure and charcoal amendments." Plant and Soil 249, 343357.

Lehmann, J., Joseph, S., 2009. "Biochar for Environmental Management: An Introduction." Biochar for Environmental Management, Science and Technology, Earthscan, London, 1-12.

Lei, O., Zhang, R., 2013. "Effects of biochars derived from different feedstocks and pyrolysis temperatures on soil physical and hydraulic properties." J. Soils Sed. 13, 15611572.

Lim, T.J., Spokas, K.A., Feyereisen, G., Novak, J.K.,2016. "Predicting the impact of biochar additions on soil hydraulic properties." Chemosphere. 142, 136-144.

Lin, Y., Munroe, P., Joseph, S., Kimber, S., Van Zwieten, L. 2012. "Nanoscale organo-mineral reactions of biochars in ferrosol: an investigation using microscopy." Plant and Soil 357, 369380.

Lopez, V.D., 2014. "Biochar as a soil amendment: Impact on hydraulic and physical properties of an arable loamy sand soil." Retrieved from: http://Www.Escholarship. Org/Uc/Item/3223673m. eScholarship, University of California. http://www.escholarship. org/uc/item/3223673m.

Liu, Z., Dugan B., Masiello, C.A., Barnes, R.T., Gallagher, M.E., 2016. "Impacts of biochar concentration and particle size on hydraulic conductivity and DOC leaching of biocharsand mixtures." Journal of Hydrology. 533, 461-472.

Madsen, M.D., Chandler, D.G., Reynolds, W.D., 2007. "Accounting for bias and boundary condition effects on Measurements of saturated core hydraulic conductivity." Soil Sci. Soc. Am J. 72:750-757.

Meyer, S., Glaser, B., Quicker, P., 2011. "Technical, economical, and climate-related aspects of biochar production technologies: a literature review. " Environmental Science & Technology. 45(22), pp.94739483.

Miyazaki, T., 2006. Water Flow in Soils (2nd ed.) Boca Raton, FL: CRC Press

Moutier, M., Shainberg, I., Levy, G.J., 2000. “Hydraulic gradient and wetting rate effects on the hydraulic conductivity of two calcium Vertisols.” Soil Sci. Soc. Am. J. 64, 12111219.

Mukherjee, A., A.R. Zimmerman, and W. Harris., 2011. “Surface chemistry variations among a series of laboratory-produced biochars”. Geoderma. 163 (3-4): 247-255.

Mukherjee, A., and Lal, R., 2014. “The biochar dilemma.” Soil Research. 52, 217-230

Oguntunde, P.G., Abiodun, B.J., Ajayi, A.E., Van de Giesen, N., 2008. “Effects of charcoal production on soil physical properties in Ghana.” J. Plant Nutr. Soil Sci. 171, 591596.

Oliviera I.B., Demond, A.H., Salehzadel A.,1996. “Packing of Sands for the Production of Homogeneous Porous Media.” Soil Sci. Soc. Am. J. 60:49-53

Ouyang, L., Wang, F., Tang, J., Yu, L., Zhang, R., 2013. “Effects of biochar amendment on soil aggregates and hydraulic properties.” J. Soil Sci. Plant Nutr. 13 (4), 9911002.

Pathan, S.M., Aylmore, L.A.G., Colmer, T.D., 2003. “Properties of several fly ash materials in relation to use as soil amendments.” J. Environ. Qual. 32, 687693.

Reddi, L.N., Xiao, M., Hajra, M.G., Lee, I.M., 2005. Physical clogging of soil filters under constant flow rate versus constant head. Can. Geotech. J. 42, 804811.

Reddy, K. R., Xie, T., and Dastgheibi, S., 2014. “Evaluation of Biochar as a Potential Filter Media for the Removal of Mixed Contaminants from Urban Storm Water Runoff.” Journal of Environmental Engineering, 140(12).

Rogovska, N., Laird, D.A., Rathke, S.J., Karlen, D.L., 2014. “Biochar impace on Mid-western Mollisols and maize nutrient availability.” Geoderma 230231, 340347.

Maharani, R., Yutaka, T., Yajima, T., and Minoru, T., 2010. “Scrutiny on physical properties of sawdust from tropical commercial wood species: effects of different mills and sawdust’s particle size.” Journal of Forestry Research Vol. 7 No. 1: 22, 20-32.

Rondon, M., Ramirez, J.A. and Lehmann, J., 2005, “Charcoal additions reduce net emissions of greenhouse gases to the atmosphere.” in Proceedings of the 3rd USDA Symposium on Greenhouse Gases and Carbon Sequestration, Baltimore, USA, p. 208.

Rogovska, N., Laird, D.A., Rathke, S.J., Karlen, D.L., 2014. "Biochar impace on Midwestern Mollisols and maize nutrient availability." Geoderma 230231, 340347.

Saquing, Jovita M., Yu-Han Yu, and Pei C. Chiu. 2016. "Wood-Derived Black Carbon (Biochar) as a Microbial Electron Donor and Acceptor". Environmental Science & Technology Letters. 3 (2): 62-66.

Schroth, M. H., et al., 1996. "Characterization of Miller-similar silica sands for laboratory hydrologic studies." Soil Science Society of America Journal 60.5: 1331-1339.

Shahabi, A.A., Das, B.M., Tarquin, A.J., 1984. "Empirical relation for coefficient of permeability of sand." In: Nat Conf Pub, Inst of Engineers, Australia, 84(2):5457

Sing, K., Everett, D., Haul, R., Moscou, L., Pierotti, R., Rouquerol, J., et al., 1985. "Reporting physisorption data for gas/solid systems with special reference to the determination of surface area and porosity." Pure Appl Chem. 57(4):603e19.

Sparkes, J. and Stoutjesdijk, P., 2011. "Biochar: implications for agricultural productivity (Report No. 11.06)." Retrieved from https://www.researchgate.net/publication/237079673Biocharimplicationsforagriculturalproductivity

Spokas, K.A., Reicosky D.C., 2009. "Impacts of sixteen different biochars on soil greenhouse gas production." Annals of Environmental Science. 3, 179-193.

Spokas, K.A., Novak, J.M., Masiello, C.A., Johnson, M.G., Colosky, E.C., Ippolito, J.A., Trigo, C., 2014. "Physical disintegration of biochar: an overlooked process." Environ. Sci. Technol. Lett. 1, 326332.

Takaya, C. A., Fletcher, L. A., Singh, S., Anyikude, K. U., & Ross, A. B., 2016. "Phosphate and ammonium sorption capacity of biochar and hydrochar from different wastes." Chemosphere, 145, 518-527.

Sullivan, R. R., and Hertel. K. L., 1942. Advances in Colloid Sci., NO. Geol, 34, 1748 (1950). 1, 37.

Tian, J., Yi, S., Imhoff, P. T., Chiu, P., Guo, M., Maresca, J. A., Beneski, V., and Cooksey, S. H.2014. "Biochar-amended media for enhanced nutrient removal in stormwater facilities." World Environmental and Water Resources Congress 2014: Water without Borders, W. C. Huber, ed., Americal Society of Civil Engineers, Portland, Oregon, 197-208.

Tian, J., Jin, J., Imhoff, P. T., Chiu, P. C., Cha, D. K., Guo, M., Maresca, J. A. "A biochar- and zero-valent iron-amended bioretention cell for enhanced nitrate removal from stormwater." Manuscript in preparation.

U.S. Salinity Laboratory, 2000. "The DISC Computer Software for Analyzing Tension Disc Infiltrometer Data by Parameter Estimation." Agriculture Research Service, U.S. Department of Agriculture. Riverside, California.

Uzoma, K.C., Inoue, M., Andry, H., Fujimaki, H., Zahoor, A., Nishihara, E., 2011. Effect of cow manure biochar on maize productivity under sandy soil condition. Soil Use Manage. 27, 205212.

Wang, C., Walter, M.T., Parlange, J-Y., 2013. Modeling simple experiments of biochar erosion from soil. Journal of Hydrology 499: 140145.

Warnock, D.D., Lehmann, J., Kuyper, T.W., Rillig, M.C., 2007. "Mycorrhizal responses to biochar in soil concepts and mechanisms." Plant and Soil 300, 920.

Webb, P.A., 2001. "Volume and Density Determinations for Particle Technologists." Micromeritics Instrument Corps.

Weibel, E.W., Kistler, G.S., Scherle, W.F., 1966. "Practical sterological methods for morphometric cytology." J Cell Biol, 30(1):23e38.

Wyllie, M.R.J., Gregory, A.R., 1955. "Fluid Flow through Unconsolidated Porous Aggregates-Effect of Porosity and Particle Shape on Kozeny-Carman Constants." INDUSTRIAL AND ENGINEERING CHEMISTRY. pg 1379.

Xu, G., Lv Y., Sun, J., Shao, H., Wei, L., 2012. " Recent advances in biochar applications in agricultural soils: Benefits and environmental implications." Clean - Soil, Air, Water 40, 1093-1098.

Yao, Y.; Gao, B.; Zhang, M.; Inyang, M.; Zimmerman, A.R., 2012. "Effect of biochar amendment on sorption and leaching of nitrate, ammonium, and phosphate in a sandy soil." Chemosphere. 89, 14671471.

Yi, S., Witt, B., Chiu, P., Guo, M., Imhoff, P., 2015. "The Origin and Reversible Nature of Poultry Litter Biochar Hydrophobicity." J. Environ. Qual. 44:963971.

Zhang, J., Chen, Q., You, C. F., 2016. Biochar effect on water evaporation and hydraulic conductivity in sandy soil. Pedosphere. 26(2): 265272.

Zimmermann, B., Elsenbeer, H., De Moraes, J.M., 2006. "The influence of land-use changes on soil hydraulic properties: implications for runoff generation." Forest ecology and management 222.1: 29-38.

Appendix A

IMAGES OF SAMPLES

Figure A.1: Sample images for soils.

From (a) to (d) are: Type 1, 3, 5 and 8, respectively. From (a) to (c) are: large biochars, small biochars, and unsieved biochars, respectively.

Figure A.2: Sample images for biochars. (a) Large biochar; (b) Small biochar; (c) Unsieved biochar

Appendix B

PHYSICAL-CHAMICAL PROPERTIES OF SOIL REEF BIOCHAR

Table B.1: Physical-chamical properties of Soil Reef biochar (Saquing, 2016). [a]Data provided by The Biochar Company unless otherwise noted. [b]Measured at the University of Delaware. (Reprinted (adapted) with permission from (Saquing, Jovita M., Yu-Han Yu, and Pei C. Chiu. 2016. "Wood-Derived Black Carbon (Biochar) as a Microbial Electron Donor and Acceptor". Environmental Science & Technology Letters. 3 (2): 62-66.). Copyright (2016) American Chemical Society.)

	Value[a]	Units	Method
pH	8.71[b]		1:20 w/v in DI water, 24hr
Electrical Conductivity	283	mmhos cm^{-1}	4.11 USCC:dil. Rajkovich
Total Ash	21.4	% of total mass	ASTM D-1762-84
Particle Density	1.816[b]	g cm^{-3}	
BET Surface Area	391±10[b]	m^2 g^{-1}	N_2 adsorption
Organic Carbon (org-C)	74.2	% of total mass	Dry Combustion-ASTM 4373
Total nitrogen (N)	0.59	% of total mass	Dry Combustion-ASTM 4373
Hydrogen/Carbon (H/C) Ratio	0.26		Dry Combustion-ASTM 4373
Liming (neutral value as CaCO3)	14.7	% $CaCO_3$	Rayment & Higinson
Total Potassium(K)	3566	mg/Kg dry mass	Enders & Lehman
Available K	4034	mg/Kg dry mass	Wang after Rajan
Total Phosphorous(P)	2528	mg/Kg dry mass	Enders & Lehman
Available P	1608	mg/Kg dry mass	Wang after Rajan
Total N	0.59	mg/Kg dry mass	KjN
Ammonia (NH4-N)	4.1	mg/Kg dry mass	Rayment & Higinson
Nitrate (NO3-N)	63	mg/Kg dry mass	Rayment & Higinson
Organic (Org-N)	5800	mg/Kg dry mass	
Chlorine (Cl)	325	mg/Kg dry mass	TMECC
Sodium (Na)	465	mg/Kg dry mass	EPA 3050B/EPA 6010

Appendix C

PROCEDURES FOR RUNNING INFILTROMETER TESTS

1. Fill apparatus with water.

a. Connect all pieces of apparatus. Close drain tube to bubbler tower (smaller column). Insert rubber stopper into top opening of this column to seal.

b. Place in pan.

c. Fill pan with tap water.

d. Connect tubing at top of reservoir (the tall column) to vacuum pump.

e. Set valve/knob at bottom of reservoir to 12 oclock position.

f. Raise air inlet tube to reservoir.

g. Use vacuum pump to fill reservoir with water.

h. Close rubber tube at top of reservoir (where vacuum was applied) with clamp.

i. Remove top cap of bubbler tower (the short column) and add water to achieve desired suction pressure setting.

j. Re-attach top cap to bubbler tower. To further lower and adjust water level in bubbler tower, remove rubber plug from top of this tower and use drain tube from bubble tower to drain water out as desired. Use small bottle to add water to bubbler tower to adjust water level (if needed).

k. When at desired water level in bubbler tower, insert rubber stopper in top opening of bubbler tower. Lower air inlet tube to reservoir to inhibit water infiltration. Turn the reservoir valve to the 3 oclock or 9 oclock position. These steps should prevent water from infiltrating from the reservoir.

2. Prepare soil surface for sampling.

a. Use scissors to cut grass, etc. so that the tension infiltrometer will be in contact with surface soil when placed.

b. Place a thin layer of fine sand on the surface of the soil to ensure good hydraulic contact. We will use 40/50 Accusand. Accusand is the manufacturer, and this sand passes the No. 40 sieve but is retained on the No. 50 sieve. Thus, particles have a narrow range of diameters.

c. Moisten the sand by spraying it with water.

3. Installing instrument and taking measurements.

a. Move the infiltrometer from its storage bucket to the soil surface.

b. Double check to make sure there are no air bubbles in the foot or base of the infiltrometer. If bubbles exist, use the air inlet tube for the reservoir to gently plunge the foot and dislodge any air without allowing water to enter the soil.

c. Double check to make sure the water suction you want to apply to the soil surface is set properly. This is the water level reading in the bubbler tower. The water level reading is the actual pressure, in mm of water, that is applied to the soil surface. Pressures are negative, and the readings in the bubbler are mostly negative.

d. Begin the infiltration experiment. Remove the rubber plug from the bubbler tower. Remove the air inlet tube from the foot or base of the infiltrometer. Turn the knob on the bottom of the reservoir to the 12 oclock position (high flow rate) or the 6 oclock position (low flow rate). Generally, I think it is best to start at the 12 oclock position and then switch to the 6 oclock position if infiltration rates are slow.

e. Once bubbling action commences, record a) the water level in the reservoir, b) the time of this measurement (minutes + seconds), and c) the water suction reading in the bubbler tower. Also record the reservoir valve setting (12 oclock or 6 oclock position).

f. Repeat step e. every few minutes.

g. Continue for approximately 30 minutes. For most real field tests I believe measurements would generally be continued for most pressure settings for 60 minutes. However, shorter measurement times are needed here to get two steady-state flow rate measurements per group.

4. Changing suction for next infiltration measurement.

a. Stop water infiltration. Insert air inlet tube into foot or base. Turn the reservoir valve so the notch is pointing to the 3 oclock or 9 oclock position. This should prevent water from infiltrating from the reservoir into the soil.

b. Keep infiltrometer in place on top of soil.

c. Follow steps in part 1 above to adjust water level in bubbler tower to desired position.

d. Record this new setting.

5. Continued water infiltration measurements.

a. Repeat steps in part 3 above for collecting data at this new water suction setting.

Appendix D

WALL EFFECT RATIO

Table D.1: Wall effect Ratio.

Type #	1	2	3	4	5	6	7	8
d_{50}(cm)	0.0809	0.0562	0.0630	0.0724	0.0541	0.0533	0.0542	0.0555
Ratio	62	89	79	69	92	94	92	90

Appendix E

DIFFERENCE BETWEEN PREDICTED AND MEASURED K_{SAT}

Table E.1: Difference between predicted and measured K_{sat}

Models	Type No.	ΔK[a]	Models	Type No.	ΔK
K-C[b]	1	100.86	Chapius	1	2.72
	2	71.81		2	1.03
	3	33.21		3	1.69
	4	89.91		4	7.06
	5	38.16		5	-0.29
	6	88.05		6	2.84
	7	79.67		7	2.53
	8	364.76		8	3.27
Hazen	1	2.81	Shahabi	1	9.83
	2	0.53		2	6.62
	3	1.63		3	3.56
	4	3.46		4	11.03
	5	1.13		5	-0.59
	6	8.28		6	3.55
	7	5.72		7	1.56
	8	2.48		8	2.48
NAVFAC	1	3.08	F-H[c]	1	15.72
	2	1.49		2	11.22
	3	3.84		3	4.74
	4	27.98		4	14.11
	5	-0.07		5	-0.02
	6	2.03		6	1.71
	7	3.68		7	1.45
	8	9.12		8	9.23

[a] ΔK has been defined in Chapter 4.
[b] A shape factor of 5 was used for Types 1 to 8.
[c] Fair Hatch: a shape factor of 6.1 and 6.0 was used for Types 1 to 4, and Types 5 to 8, respectively.

.

Appendix F

SOIL WATER REPELLENCY TESTS

An important biochar property is wettability and its effects in soil water repellency has been receiving attention recently. Water repellent soils do not wet spontaneously when water is dropped on the surface. As soil water repellency affects infiltration, evaporation and many other soil hydrologic properties (Leelamanie *et al.,* 2010), understanding biochar wettability is very useful in engineering application. During the development of a K_{sat} measurement involving biochar, we found that it is extremely hard to fully saturate soils with biochar amendment if they were wet-packed. It was postulated that biochar surface is repellent to water thus made it difficult to achieve fully saturation.

Many techniques such as water drop penetration time test (WDPT), the morlarity of an ethanol droplet (MED) test, the ninety-degree surface tension method and thermal analysis etc. have been developed to measured the water repellency of soils. The most common two ways to characterize the magnitude of water repllency are the WDPT and liquid-solid contact angle (CA) measurement (Leelamanie *et al.,* 2010).

F.1 Water Drop Penetration Test

The WDPT test has been considered as the most indicative hydrological consequences of water repellency (Doerr, 1998). It consists of placing a water droplet on the soil surface and measuring the time until complete penetration (Leelamanie *et al.,* 2010). Unsieved SR550 biochar samples (5 g) were placed in a 25-ml dish. Yi etal. showed that the WDPT did not very between 10-, 30-, and 50- μL droplets in their initial tests, therefore 10-μL DI water droplets were used in this study. For each sample, 5 to 10 droplets were sequentially placed on dry region of the soil surface with a burette at a height of about 10 mm, and the time to completely penetrate the sample surface was recorded(Yi *et al.,* 2015; Leelamanie *et al.,* 2010). Samples with WDPT $\leq$5 s were considered nonrepellent, 5-60 s slightly repellent, 60-600 s strongly water repellent, 600-3600 s severely repellent and $\geq$ 3600 s extremely repellent (Bisdom *et al.,* 1993). The air temperature was 22.6 °C with 19% relative humidity (RH).

It was found that WDPT were less than 5s for soil reef biochars, which indicates a strong nonrepellent property.

F.2 Contact Angle Test

A sessile drop contact angle method has been developed by Bachmann etal. to access soil water repellency. Unlike WDPT, which is an indirect measurements of soil wettability, CA measurements directly quantify the effects of solid surface properties on the distribution and morphology of water in porous media (Bachmann *et al.,* 2000). RH was 19 to 21% and temperature ranged from 21 to 22.3 °C for all measurements. Following the protocol developed by Leelamanie etal. and Yi etal. of sample preparation for CA test, firstly the microscope slides were washed with 1 % nitric acid, dried at 105 °C and cooled to room temperature. A double-sided adhesive tape (Scotch Removable Double Sided Tape, 3M Co.) with an area of about 4 cm^2 was placed on the slide to affix the particles. Sample particles were sprinkled on the adhesive tape, and then it was pressed to the tape with a 100-g weight for 10 s, followed by tapping the slide to remove surplus particles. Repeat the procedure until the tape is all covered with particles. Triplicated slides were prepared for each sample, and CA was measured at the three-phase contact line on three to four water droplets on each slide using a goniometer fitted to a microscope (NRL CA Goniometer model no. 10000155, Rame-hart, Inc.).

For the sake of comparison, accusand was treated by heating under 550 °C for 24 hr after rinse, and another set of accusand was dried under 90 °C overnight after rinse. Figure F.1 illustrates the results from CA test. Dried Accusand has a CA of 28 ° at the beginning, and after 600+ s, the reading became approximately 4 °. Heated accusand

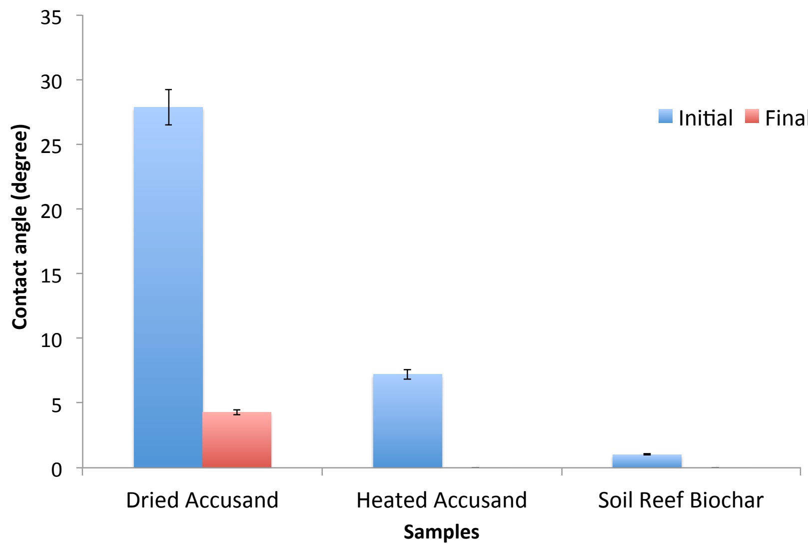

Figure F.1: Contact angle tests.

has a smaller CA of 8° and then it became 0 after some time. Soil reef biochar has a very low CA compared to dried and heated accusand.Those results, again, indicate that soil reef biochar is highly hydrophilic.

Appendix G

PERMISSION LETTERS

Permission Letter to Use Copyright Info Inbox x

Ray.Lombardi@micromeritics.com
to me, tony.thornton, tom.cook

Dear Jing Jin,

Thank you for your request to use our copyrighted information.

We would be happy to cooperate with you.

In order to use these figures we require in addtion to your citation reference, a copyright statement. It should include this information:

Copyright owned by Micromeritics Instruments. Information or figures may not be reproduced or used in any manner without written permission of Micromeritics.

Ray Lombardi

micromeritics®
The Science and Technology of Small Particles™

Ray Lombardi
Director of Marketing
Micromeritics Instrument Corp.
4356 Communications Drive
Norcross, GA 30093
P: (770) 662-3671
C: (404) 434-1827
www.micromeritics.com

You Tube

Watch us Follow us

Jing Jin wrote:
From: Jing Jin <jinjing@udel.edu>
To: mas@particletesting.com,
Cc: orders@micromeritics.com
Date: 04/17/2016 11:40 AM
Subject: Permission Letter

Figure G.1: Permission for use of Figure 3.1 and Figure 3.2

American Water Works Association

Dedicated to the World's Most Important Resource™

6666 West Quincy Avenue
Denver, CO 80235-3098
T 303.794.7711
www.awwa.org

April 22, 2016

Ms. Jing Jin
121 Thorn Lane, Apt 9
Newark, Delaware

Dear Ms. Jin:

We are pleased to grant permission to reproduce the following AWWA material:

> Figure 2 from *Fundamental Factors Governing the Streamline Flow of Water Through Sand [with discussion]*, *Journal AWWA*, Vol 25, Issue 11, Nov. 1933, page 1556.

Reproduction is authorized for the following stated purpose:

> To be included in thesis titled, *Predicting Changes in Saturated Hydraulic Conductivity of Bioretention Media Amended with Biochar,* and posted electronically to be accessible by the research community called ProQuest ETD Administrator.

Please use the following citation when you credit AWWA:

> Reprinted from *Journal AWWA, Vol. 25*, by permission. Copyright © 1933 American Water Works Association.

Thank you for your attention to this matter.

Sincerely,

Director of Publishing
ZS/ng

Figure G.2: Permission for use of Figure 4.10

Copyright Clearance Center RightsLink® Home Create Account Help Live Chat

ACS Publications Most Trusted. Most Cited. Most Read.

Title: Wood-Derived Black Carbon (Biochar) as a Microbial Electron Donor and Acceptor

Author: Jovita M. Saquing, Yu-Han Yu, Pei C. Chiu

Publication: Environmental Science & Technology Letters

Publisher: American Chemical Society

Date: Feb 1, 2016

LOGIN

If you're a copyright.com user, you can login to RightsLink using your copyright.com credentials. Already **a RightsLink user** or want to learn more?

PERMISSION/LICENSE IS GRANTED FOR YOUR ORDER AT NO CHARGE

This type of permission/license, instead of the standard Terms & Conditions, is sent to you because no fee is being charged for your order. Please note the following:

- Permission is granted for your request in both print and electronic formats, and translations.
- If figures and/or tables were requested, they may be adapted or used in part.
- Please print this page for your records and send a copy of it to your publisher/graduate school.
- Appropriate credit for the requested material should be given as follows: "Reprinted (adapted) with permission from (COMPLETE REFERENCE CITATION). Copyright (YEAR) American Chemical Society." Insert appropriate information in place of the capitalized words.
- One-time permission is granted only for the use specified in your request. No additional uses are granted (such as derivative works or other editions). For any other uses, please submit a new request.

If credit is given to another source for the material you requested, permission must be obtained from that source.

BACK CLOSE WINDOW

Figure G.3: Permission for use of Table B.1